

AGCM Precipitation Biases in the Tropical Atlantic

M. BIASUTTI

Lamont-Doherty Earth Observatory, Columbia University, Palisades, New York

A. H. SOBEL

Department of Applied Physics and Applied Mathematics, and Department of Earth and Environmental Sciences, Columbia University, New York, New York

Y. KUSHNIR

Lamont-Doherty Earth Observatory, Columbia University, Palisades, New York

(Manuscript received 24 May 2005, in final form 12 September 2005)

ABSTRACT

Many general circulation models (GCMs) share similar biases in the representation of the intertropical convergence zone (ITCZ) in the Atlantic, even when they are forced with the time series of the observed sea surface temperature (SST). Specifically, they overestimate precipitation in the Southern Hemisphere in boreal spring and in the Caribbean region in boreal summer.

The majority of the models considered here place the rainfall maximum over the SST maximum, although the true precipitation maximum does not occur there. This is the case even though these GCMs accurately place the maximum in surface wind convergence away from the SST maximum, at the location where the observed precipitation maximum lies.

Models that overrespond to SST in this way tend to (i) have fewer heavy-rain events, (ii) rain more for a smaller amount of water vapor in the atmospheric column, and (iii) couple rainfall and surface humidity too strongly and rainfall and humidity above the surface too weakly.

1. Introduction

Our ability to predict rainfall in such climate-sensitive areas as the Gulf of Guinea, Sahel, and Northeast Brazil is contingent on our ability to predict the evolution of SST in the tropical Atlantic (Goddard and Mason 2002). Unfortunately, our coupled models are woefully deficient in this regard (Goddard et al. 2001; DeWitt 2004).

Such deficiency may derive from a model's inability to reproduce the annual cycle of precipitation and SST in the tropical Atlantic (Huang et al. 2004; Biasutti 2000) and, indeed, most current coupled models fail to reproduce even the gross features of the Atlantic ITCZ/cold tongue complex (Davey et al. 2002).

Though exacerbated in coupled models, some of

these biases are already present in simulations of the atmospheric model with prescribed SST or coupled to a flux-adjusted slab ocean model. For example, in most atmospheric GCMs, the Atlantic marine ITCZ (AMI) reaches well into the Southern Hemisphere, contrary to what is observed. The prevalence of this kind of bias underscores our incomplete understanding of what controls the location of precipitation over the tropical oceans and warrants a thorough investigation.

If we take the view that convection is to first order the release of an instability of the atmospheric column, then we expect the ITCZ location and intensity to be determined by environmental conditions, such as the vertical distribution of moisture and temperature, SST, and air-sea heat and moisture exchange. Atmospheric GCMs are constructed to simulate all these aspects of the problem through a combination of parameterized and explicit processes, and yet the simulations are deficient. There could be several reasons for a model's shortcomings in representing the AMI, but it is useful to posit two simple scenarios: (i) the large-scale envi-

Corresponding author address: Michela Biasutti, Lamont-Doherty Earth Observatory, Columbia University, 61 Route 9W, P.O. Box 1000, Palisades, NY 10968-8000.
E-mail: biasutti@ldeo.columbia.edu

ronmental conditions to which the convection responds are unrealistic due to systematic errors in the large-scale circulation that can be viewed as external to the convection (e.g., the characteristics of air masses advected into the AMI from the Sahara might be biased), or (ii) the model convection scheme (or other parameterized physics) responds incorrectly to the large-scale environment (e.g., the Saharan air layer might be well represented, but the convective parameterization might be too insensitive to the presence of dry air at the top of the boundary layer). While reality, in many models, is probably a more complex situation in between these two extremes, because of strong feedbacks between the convection and its environment and between different physical parameterizations, we find the simple partitioning between environment and convective response to be conceptually useful.

Our long-term goal is to identify whether biases arise from an unrealistically simulated large-scale environment, from parameterization errors, or from some complex interaction between the two. If parameterization errors are involved as seems likely we aim to gain some insight into how the parameterizations might be improved. The scope of this study is more limited: first, we present an overview of the biases in the annual cycle of tropical Atlantic precipitation in several widely used AGCMs; second, we diagnose the relationship between precipitation and several environmental variables, comparing our findings for the models with current theories and observations of the ITCZ. We highlight common behaviors in models with common biases in precipitation and thus identify to what atmospheric properties precipitation is most sensitive in such models.

The paper is organized as follows. Section 2 presents a short description of the datasets. Section 3 gives an overview of precipitation biases in the tropical Atlantic. Section 4 describes the simulated large-scale environment. Section 5 diagnoses the relationship between convection and the environment. Section 6 draws our conclusions and makes suggestions for model development.

2. The datasets

For comparison to the models' precipitation, we use the Climate Prediction Center (CPC) Merged Analysis of Precipitation (CMAP) (Xie and Arkin 1997), Global Precipitation Climatology Project (GPCP) (Adler et al. 2003), and Arkin and Janowiak Geostationary Operational Environmental Satellite (GOES) Precipitation Index (GPI) data (available online at ftp://lake.nascom.nasa.gov/data/TRMM/Ancillary/3A44/README_gpi_pentad) and precipitation estimate using microwave-calibrated IR [from now on Tropical Rainfall Measur-

ing Mission (TRMM) data; Adler et al. 2000] datasets. The climatology is calculated over the 1980–2001 period in the former two datasets and over the 1998–2003 period in the latter. Other observational gridded datasets used in this study are Reynolds SST (Reynolds and Smith 1994), TRMM SST (Wentz et al. 2000) and precipitable water, QuickScat surface winds (Graf et al. 1998), and surface fluxes climatologies from the Southampton Oceanography Center (Josey et al. 1998; Oberhuber 1988; Da Silva et al. 1994). Given the absence of upper-air data in the AMI region, we use sounding data from the two Caribbean islands and one coastal site in South America taken from the comprehensive Aerological Reference Data Set (CARDS; Eskridge et al. 1995) and daily gauge precipitation at the same stations from the World Meteorological Organization (WMO) dataset through the International Research Institute for Climate Prediction (IRI) data library (available online at <http://iridl.ldeo.columbia.edu>).

We use the reanalysis datasets both in lieu of upper-air observations over the ocean and because they represent an intermediate stage between the observations and the Atmospheric Model Intercomparison Project (AMIP)-like simulations. We present data from both National Centers for Environmental Prediction (NCEP) reanalyses [NCEP–National Center for Atmospheric Research (NCAR) Reanalysis 1 (Kalnay et al. 1996), hereafter NCEP1; NCEP Reanalysis 2 (Kanamitsu et al. 2002), hereafter NCEP2] and the European Centre for Medium-Range Weather Forecasts (ECMWF) 40-yr Re-Analysis (ERA-40) (Simmons and Gibson 2000). Climatologies are calculated over the 1980–2001 period.

We analyze output from three versions of the NCAR atmospheric model [Community Climate Model 3 (CCM3), Community Atmospheric Model 2 (CAM2), and CAM2 with the relaxed Arakawa–Schubert convective parameterization (CAM2wRAS)];¹ the ECHAM model [an offspring of the ECMWF model, modified in Hamburg by Max-Planck Institute (MPI) scientists]; National Aeronautics and Space Administration's (NASA's) Seasonal to Interannual Prediction Project atmospheric model (NSIPP); and two models developed at the Geophysical Fluid Dynamics Laboratory (GFDL_AM2, version 2 of the atmospheric model, and GFDL_R30, an older coupled model).

¹ Because we only have a subset of variables for CAM2 and CAM2wRAS integrations, we will switch back and forth between the two models in the subsequent analyses. The biases in March and September climatological rainfall patterns in CAM2wRAS are similar to those of CCM3 and CAM2 and will not be shown.

TABLE 1. List of GCMs used in this study, of the kind of convective parameterization, according to Arakawa (2004), and relevant references.

Model	Resolution	Convection	General reference	Convection reference
CCM3	T42 L18	Relaxed adjustment ($Z-M$); mass flux (H)	Kiehl et al. (1998)	Zhang and McFarlane (1995); Hack (1994)
CAM2	T42 L26	Relaxed/triggered adjustment ($Z-M$); mass flux (H)	Kiehl and Gent (2004)	Zhang and McFarlane (1995); Hack (1994)
CAM2wRAS	T42 L26	Relaxed adjustment (RAS); mass flux (H)	Kiehl and Gent (2004)	Moorthi and Suarez (1992); Hack (1994)
ECHAM4.5	T42 L19	Mass flux and relaxed adjustment	Roeckner et al. (1996)	Tiedtke (1989); Nordeng (1994)
NSIPP	$2.5^\circ \times 2^\circ 34L$	Relaxed adjustment (RAS)	Baumeister et al. (2000)	Moorthi and Suarez (1992)
GFDL_AM2	$2.5^\circ \times 2^\circ 24L$	Relaxed adjustment (RAS)	Anderson et al. (2004)	Moorthi and Suarez (1992)
GFDL_R30 (coupled; flux adjusted)	R30 ($3.75^\circ \times 2.25^\circ$) L14	Instantaneous adjustment	Delworth et al. (2002)	Manabe et al. (1965)

Table 1 provides a list and summary description of the GCMs analyzed in this study. For each model, we list the resolution, the kind of convective parameterization used by the model [following the classification provided by Arakawa (2004)], and the relevant references. All AGCM simulations use observed SST as boundary condition (AMIP-like integrations), with the exception of CAM2wRAS, which was integrated with repeating climatological SST. Besides the AGCMs, we also show some results from the old GFDL_R30 coupled model, which is flux adjusted to reproduce the observed SST. In this case we calculate the climatology from 20 yr in the middle of the control coupled integration.

To verify that our results do not depend on the use of AMIP-style integration, we have also analyzed integrations of CCM3 coupled to a slab ocean model (Biasutti et al. 2005) and the fully coupled NSIPP (available online at http://nsipp.gsfc.nasa.gov/data_req/coupled/docs/exp036_info.html) and GFDL models (Delworth et al. 2006). The question of whether the use of an uncoupled, AMIP-like simulation is appropriate for our scope stems from the work of Kumar and Hoerling (1998), among others, who have shown how imposing observed SST as boundary conditions for AGCM integrations might lead to positive precipitation biases in warm-pool regions, such as the Indian Ocean, where high SST is forced by—not a forcing to—the atmosphere. Obviously, this could be a problem in the Atlantic as well, especially in the Caribbean, where SST is warm and precipitation is weak.

In partially coupled integrations (specifically, of CCM3 coupled to a motionless slab ocean model of constant 50 m depth that is flux-adjusted to reproduce the observed SST), the annual cycle of precipitation is indistinguishable from that in uncoupled integrations, which suggests that AGCM biases do not stem from the way boundary conditions are specified. Similar conclu-

sions are drawn from a comparison of coupled and uncoupled versions of the NSIPP and GFDL models. Climatologies are modified by the coupling, but the overall characteristics of the biases are not. For example, both the coupled and uncoupled NSIPP models erroneously simulate net vertically integrated moisture convergence in the Caribbean; similarly, a tendency for a southern ITCZ in boreal spring is present in the uncoupled models and exacerbated in their coupled versions.

3. The simulated annual cycle of precipitation

a. The monthly mean climatology

Figure 1 shows the annual march of the ITCZ in the central Atlantic (averaged over two grid points around $30^\circ W$) in observations, reanalyses, and the models. The observations show the oft-noted Northern Hemisphere preference of the ITCZ. The main axis of the AMI moves as far north as $8^\circ N$ in September and stays north of the equator all year around, although the ITCZ does widen into the Southern Hemisphere in boreal spring and as far north as $14^\circ N$ in late summer.

The most recent reanalyses (NCEP2 and ERA-40) capture the meridional movement of the ITCZ quite well. The ERA-40 simulation does particularly well compared to NCEP2 during January through April: at this time, NCEP2 precipitation extends too far south. Both datasets grossly overestimate the intensity of precipitation all year round.²

The NCEP1 reanalysis and, to different extents, the AGCMs have all the same bias: they simulate an annual

² The ERA-40 Web site explains that excessive precipitation after 1991 is due to the assimilation of water vapor from satellite: the model rejects the observed values, and gets rid of what it considers excessive moisture by precipitating it out.

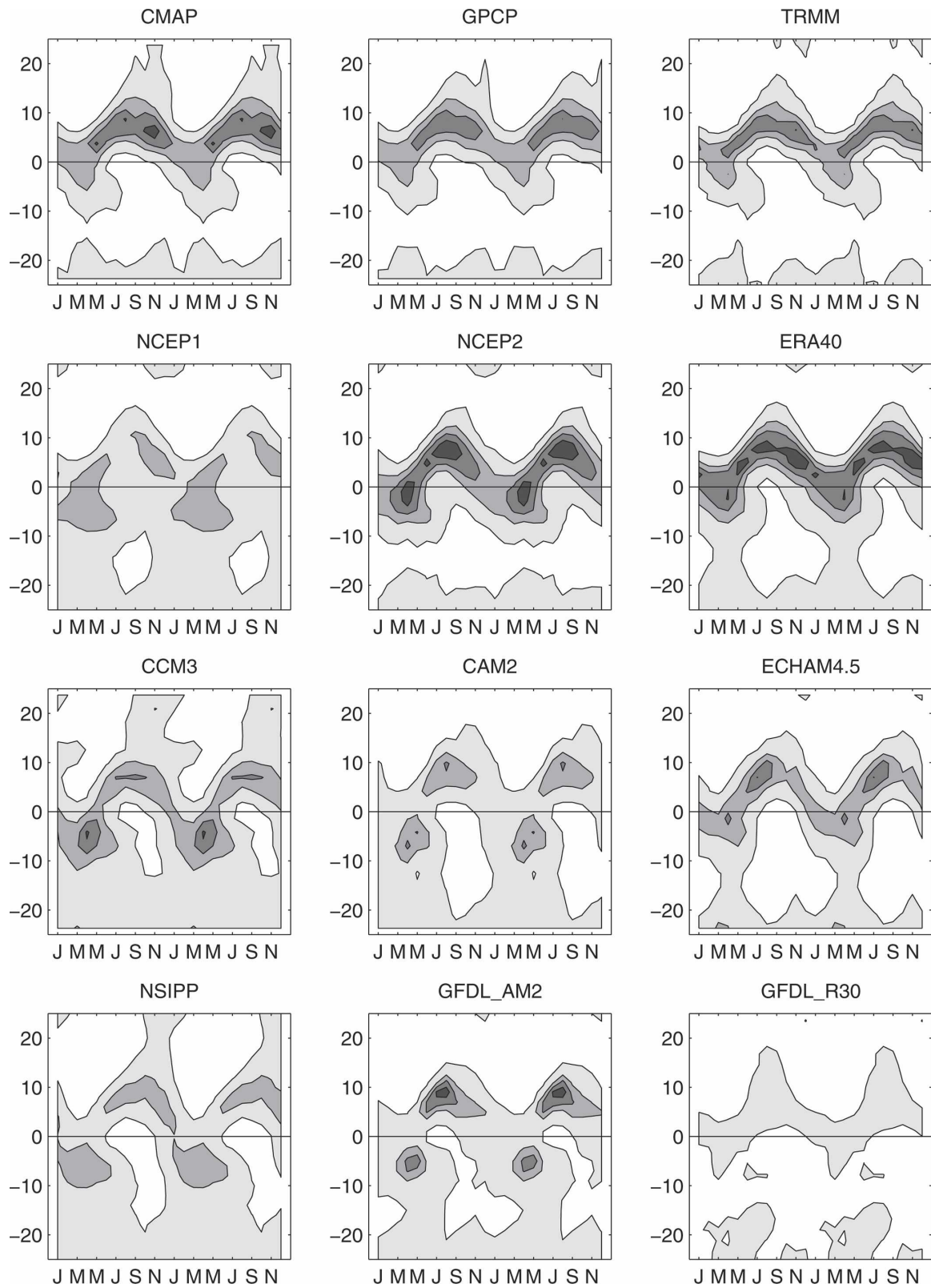


FIG. 1. The annual march of the central Atlantic (30°W) ITCZ in (top row) observations, (second row) reanalyses, and (third and bottom rows) models. The shading interval is 4 mm day⁻¹, starting with 1 mm day⁻¹; darker shading indicates more intense rainfall.

march of the AMI that is too symmetric about the equator, with a broad maximum of precipitation in the Southern Hemisphere during the first half of the year. Most models also tend to underestimate the maximum in precipitation intensity during boreal summer and fall, which makes for very little annual variation in the ITCZ intensity. ECHAM4.5, while not immune to these problems, is only weakly affected by them: spring precipitation is close to the equator and is weaker than summer precipitation (but note that fall precipitation is underestimated). The GFDL_R30 captures the northern preference of the AMI quite well, but dramatically underestimates its intensity.

Figures 2 and 3 show the climatological SST and precipitation in March and September, respectively. Two points can be made from these figures. The first is that substantial precipitation is limited to regions of SST warmer than about 27° or 28°C ; this is the reason behind the common statement that maximum precipitation is collocated with maximum SST. The second point is that a closer examination of the zonal asymmetries in the observed fields indicates that the maxima of precipitation and SST are in fact not coincident in the Atlantic. In March, precipitation is maximum on the equator, offshore of South America, while SST is maximum in the Gulf of Guinea and 1°C colder in the western basin (where the local maximum is at 5°S). Similarly in September, precipitation is maximum in the eastern basin, off the Guinea Coast, while SST is maximum in the west Atlantic and in the Caribbean Sea.

The NCEP2 and ERA-40 reanalyses capture the offset between the precipitation and SST maxima. ERA-40, in particular, seems to reproduce even details, such as the northward tilt of the ITCZ west of 30°W in September, and the equatorial maximum in March. As noted before, NCEP2 brings the March ITCZ a little too far south, closer to the local SST maximum.

The NCEP1 reanalysis and the models (again, with the partial exception of ECHAM4.5 and the GFDL_R30 model) do not reproduce the observed relationship between SST and precipitation. Instead, the simulated precipitation closely mimics the pattern of the prescribed SST. This induces the common problem of a southern ITCZ in boreal spring and of excessive rainfall in the Caribbean. As mentioned in section 2, the fact that (i) ECHAM seems immune to this bias and (ii) a version of CCM3 coupled to a slab ocean model shows the same bias as its uncoupled counterpart seems to indicate that this problem does not arise from the AMIP-style integration, but is most likely a consequence of the physics employed by the atmospheric GCMs.

Another view of the rainfall biases is given in Figs. 4

and 5, which show the difference between the GCM integrations and the CMAP dataset in March and September. In March, the models rain too little on the equator and, in most cases, too much south of the equator. In September, they rain too little in the eastern half of the basin and, in most cases, too much in the western half.

Figure 6 shows the annual cycle of precipitation and evaporation in the Caribbean region (defined as the region 10° – 25°N , 80° – 60°W). All reanalyses and AGCMs overestimate the precipitation in the region by a factor ranging from 50% (ECHAM4.5) to 150% (CCM3). The GFDL_R30 model underestimates it during summer and fall, and overestimates it during spring. Even more disturbingly, all reanalyses and two of the AGCMs (CCM3 and NSIPP) have precipitation exceeding evaporation during the Caribbean rainy season. In the case of the AGCMs, this means a bias in the large-scale circulation: they simulate net moisture convergence ($P > E$) in the Caribbean, while the observations show that this region is either near radiative-convective equilibrium ($P = E$) or a source of moisture ($E > P$). Moisture convergence into the warm pool in the Caribbean supports a maximum in rainfall in this part of the basin, likely at the expense of the ITCZ in the east.

Note that we cannot infer a convergence bias in the case of the reanalyses, because in their case moisture is not necessarily conserved [e.g., A. M. Mestas-Nunez (2005, personal communication) shows that NCEP1 simulates moisture divergence out of the Caribbean, at the same time that $P - E$ is positive].

b. The daily precipitation

Up to this point, we have focused on the biases in the monthly mean precipitation; in the remainder of the section, we show how the models reproduce the variability of daily rainfall in the AMI.

Figure 7 shows the distribution of daily rainfall for grid points in the AMI region (specifically, days 180–365, from 2° to 10°N). In the GPI dataset, 60% of the days show less than 3 mm of accumulation; 10% of the days accumulate between 3 and 6 mm, and larger precipitation is distributed over a wide range of values (with episodes of more than 30 mm of rainfall in one day). This distribution is reproduced to different degrees by all datasets. Some datasets (NCEP1, CCM3, GFDL_AM2, ERA-40) produce a distribution that is too uniform. Some fail to extend the tail of the distribution to high enough values (NCEP1, CCM3, GFDL_AM2, CAM2wRAS, CAM2). NCEP2 and ECHAM4.5 reproduce the observed distribution with good accuracy.

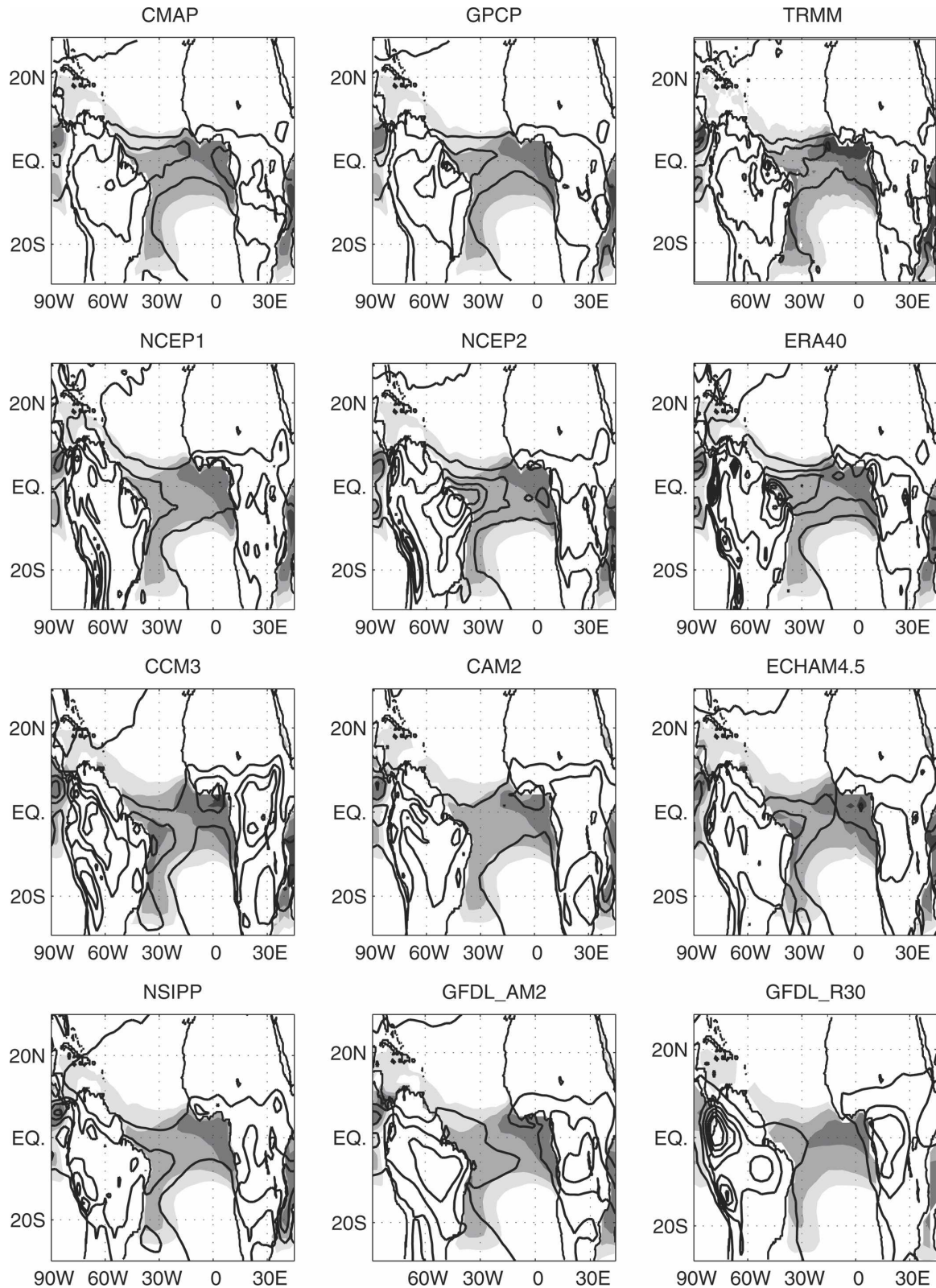


FIG. 2. The climatological March SST (shaded, the shading interval is 1°C, starting with light shading at 26.5°C and getting darker for warmer SST) and precipitation (contours, the contour interval is 4 mm day⁻¹; the first contour, which delineates the ITCZ, is the 2 mm day⁻¹ isoline). The Reynolds SST dataset is used in the CMAP and GPCP panels, TRMM SST is used in the TRMM panel, and the surface temperature field for each model is used in the other panels.

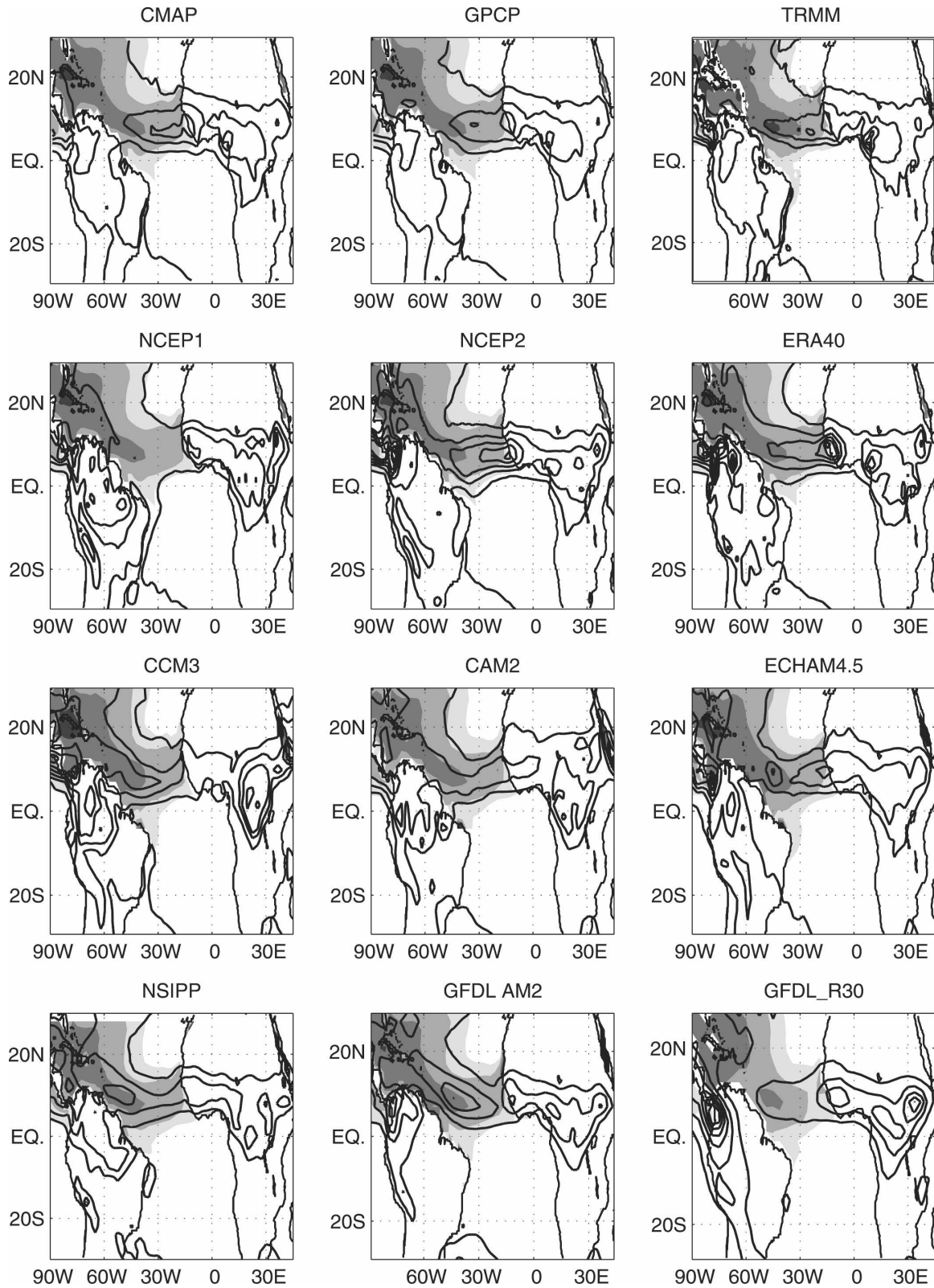


FIG. 3. As in Fig. 2, except for September.

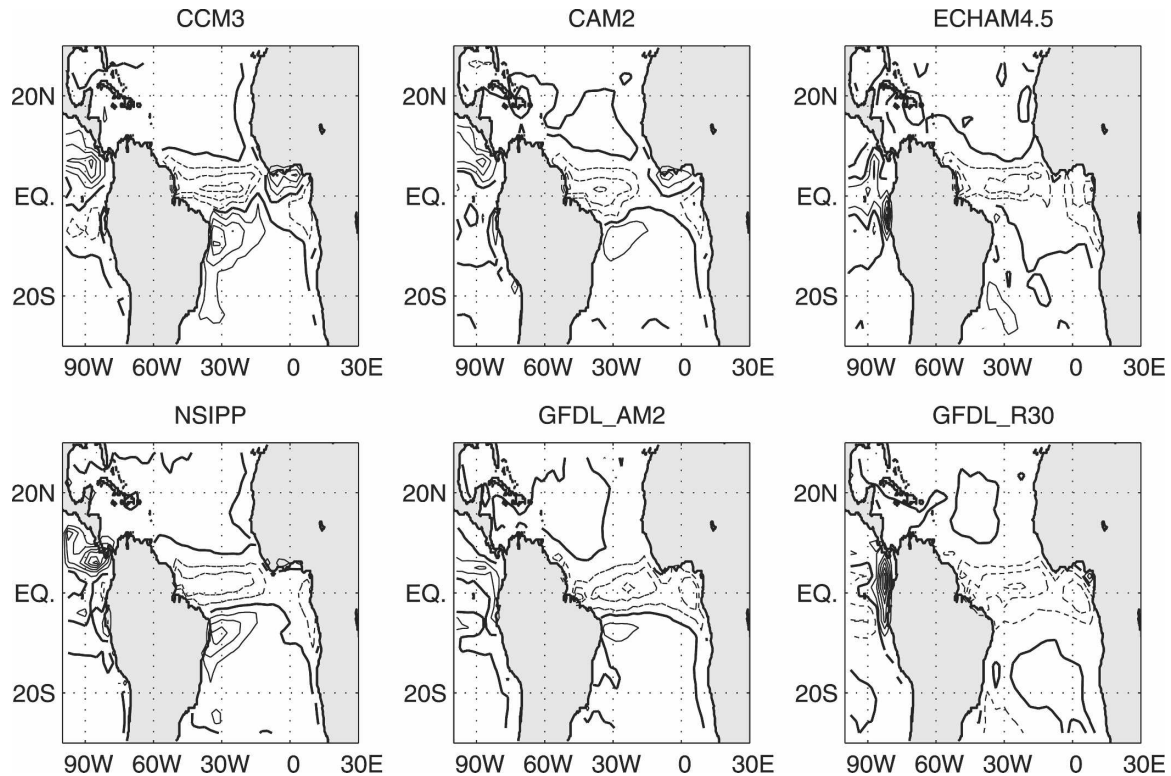


FIG. 4. The difference between climatological March precipitation in the models and the CMAP dataset (the contour interval is 2 mm day^{-1} ; negative contours are dashed; the zero line is thick).

Is there a consistent relationship between biases in the distribution of daily rainfall and biases in the monthly mean? For example, do models that underestimate the frequency of heavy-rain events underestimate the monthly accumulation? Unfortunately, there is not such a simple and consistent correspondence. For example, AM2 does not simulate days with very heavy rainfall, but reproduces the maximum intensity of the summer ITCZ quite well; GFDL_R30 model instead has heavy-rain days, but a disproportionate percentage of drizzle days, and a weak monthly mean ITCZ. Similarly, the daily rainfall distribution is too flat in both ERA-40 and NCEP1, but the former overestimates AMI monthly rainfall, while the latter underestimates it.

The only consistent relationship between daily distribution of rainfall and monthly biases seems to be the following one: models in which precipitation is more a slave to SST (i.e., in which the maximum in precipitation and the maximum in SST coincide) have a reduced range in daily precipitation. We will return to this in following sections.

The temporal characteristics of daily rainfall are diagnosed in Fig. 8, which shows the autocorrelation of daily precipitation computed for each grid point in the

AMI region (2° – 12° N during May–December) and then averaged over the grid points. In the GPI dataset, autocorrelation drops to less than 0.3 for a one-day lag and stays around 0.2 for longer lags. Such a sharp drop in autocorrelation is confirmed in station data in the Caribbean and French Guiana and is captured fairly accurately by the reanalyses. Instead, the AGCMs grossly overestimate the autocorrelation at all lags (CAMwRAS less than the others); only the GFDL_R30 reproduces the short decorrelation time (the moist convective adjustment used in this model to parameterize convection is known for producing so-called popcorn convection). A spectral analysis of daily precipitation (not shown) confirms that the models underestimate the high-frequency variability, and simulate an excessively red time series.

4. The large-scale environment

In this section, we give an overview of the large-scale environment simulated by the reanalyses and the models in the tropical Atlantic. Because the models are designed to be physically consistent and to reproduce the basic balances that one sees in nature, we expect to see biases in the large-scale environment that are consistent with the biases in precipitation. For example,

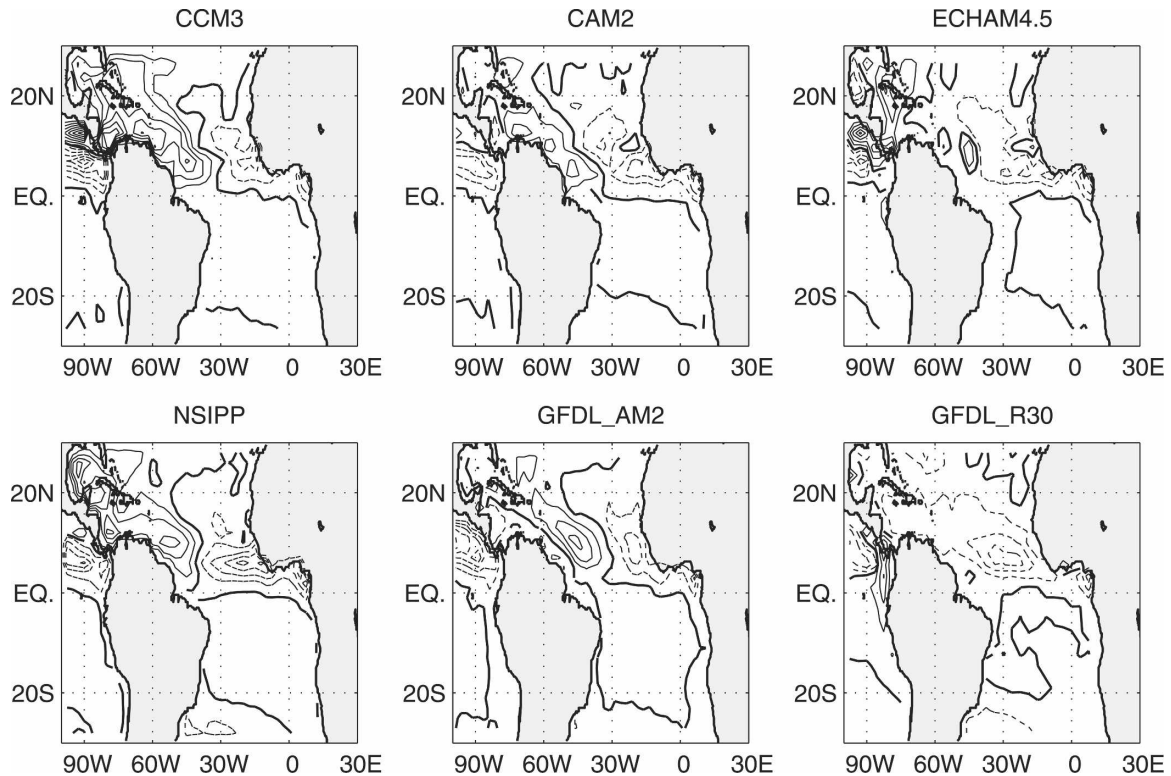


FIG. 5. As in Fig. 4, except for September.

conservation of moisture will prescribe that the column-integrated moisture convergence will be equal to precipitation minus evaporation ($P - E$). Similarly, condensational heating exceeding radiative cooling will be associated with large-scale ascent; the stronger the precipitation, the stronger the ascent. Moreover, precipitation centers in the Tropics have a large effect on the global circulation, and whatever bias we see in the latter might very well be a consequence as much as a cause of biases in the former. Thus, in most cases, when we look at the large-scale environment, we can point only to consistency, not to causality. That said, we can glean some clues about mechanisms from features of the large-scale environment that, while not inconsistent with, are not expected from the precipitation biases described in section 3.

Figure 9 shows the surface mass convergence during September; precipitation is superimposed on it for reference. The observations and the reanalyses show that substantial precipitation (say, larger than 4 mm day^{-1}) is associated with surface mass convergence. Interestingly, the models have an easier time simulating the convergence than the precipitation: even the models that put the precipitation maximum in the Caribbean do a very good job at simulating the maximum convergence off the African coast. The ability of the models to

generate the correct surface winds even as they bias precipitation suggests that—at least in this region and in this season—surface wind may be forced more directly by SST gradients [as in the Lindzen and Nigam (1987) model] than by free-troposphere heat sources.

The simulated relationship between surface convergence and precipitation is important in determining what factors control precipitation in the models. Current theories of tropical precipitation can be organized in two broad classes. In one class (e.g., Holton et al. 1971; Charney 1971; Lindzen 1974; Lindzen and Nigam 1987; Waliser and Somerville 1994; Tomas and Webster 1997; Tomas et al. 1999) the convergence of the low-level winds determines the location and intensity of precipitation. The SST enters the picture through its control on the winds via the momentum budget, which, in some cases (e.g., Lindzen and Nigam 1987), can be evaluated without any knowledge of the convective heating associated with precipitation. We will call this mechanism “dynamic control” of precipitation. In the other class (e.g., Emanuel et al. 1994; Sobel and Bretherton 2000; Raymond 2000; Raymond et al. 2003; Neelin and Held 1987; Neelin 1997; Neelin and Su 2005), precipitation is determined locally by the SST and related thermodynamic factors (such as boundary layer entropy or moist static energy). In this latter view,

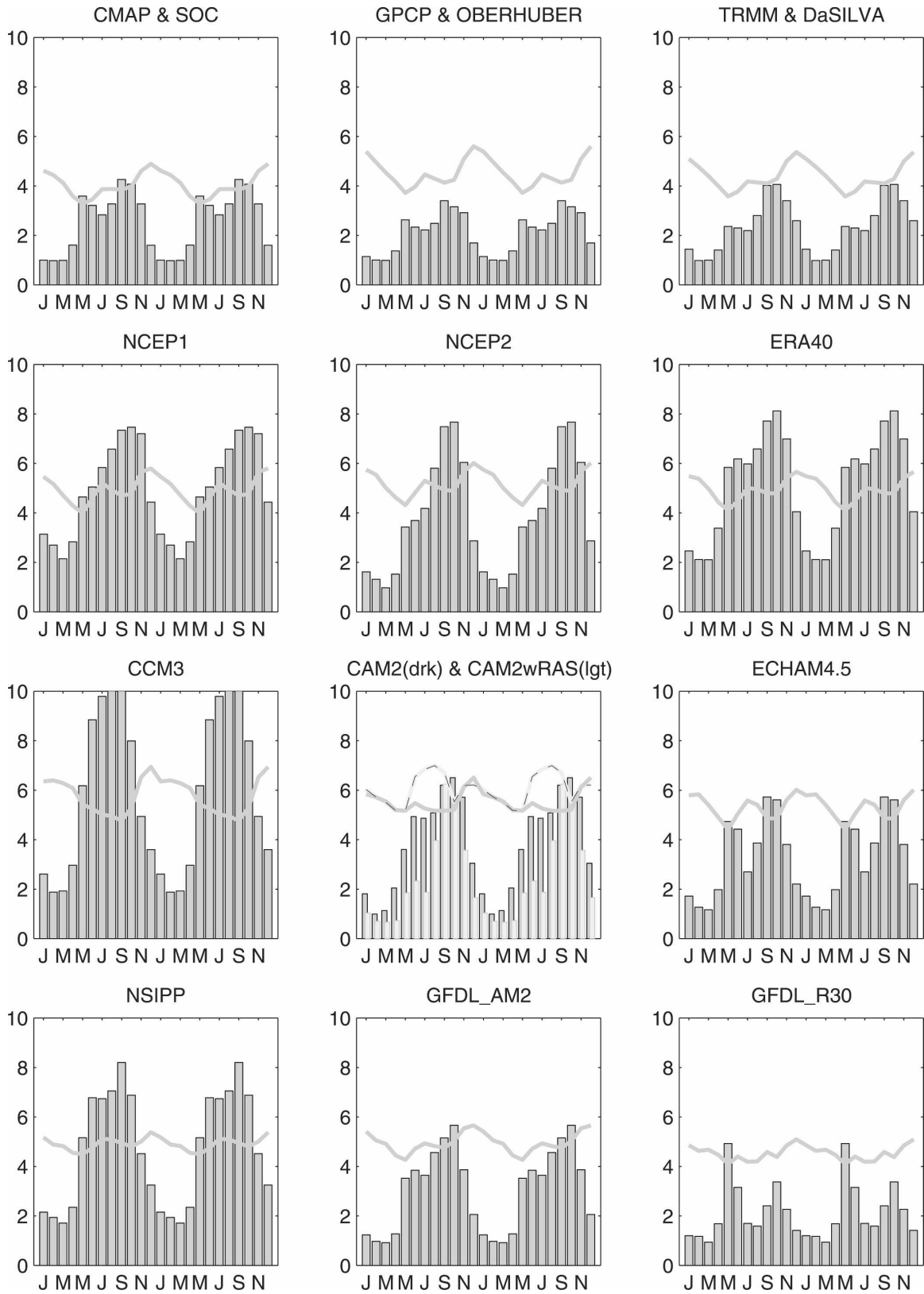


FIG. 6. The annual cycle of precipitation (bars) and evaporation (line) averaged over the Caribbean region (10° – 25° N, 80° – 60° W). The annual cycle is repeated twice.

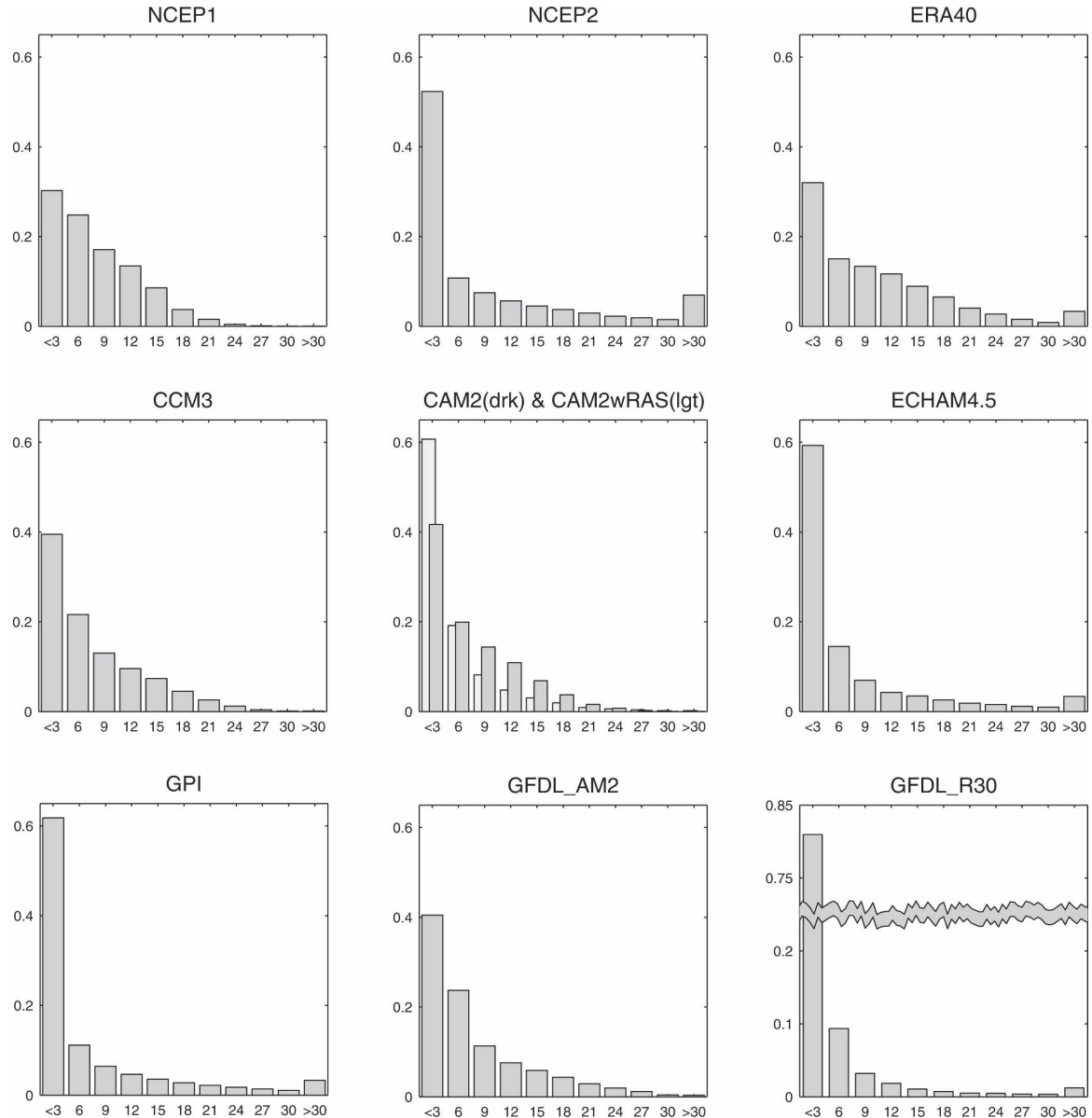


FIG. 7. Normalized distribution of daily rainfall in the AMI region (2° – 10° N across the span of the Atlantic, calculated on days 180–365). Each bar represents the fraction of data points with accumulation falling in each category: 0–3, 4–6, . . . , >30 mm.

surface convergence is either secondary in importance, or a consequence of (rather than an external forcing for) precipitating convection. We will call this mechanism the “thermodynamic control” of precipitation.

Thus, the failure of some models to overlap surface convergence and precipitation would seem to indicate that these models (which have the worst bias in precipitation) weigh the thermodynamic control of convection disproportionately more than the dynamic control, while both means of control would seem to have a role in determining the location of the observed ITCZ. A quantitative assessment of the relative role of dynamics

and thermodynamics in controlling convection in the ITCZ is beyond the scope of this paper.

The pattern of column moisture convergence strictly mimics the precipitation field (not shown). Thus, the disconnect between surface convergence and precipitation seen in some models (but not in observations) indicates a mistaken relation between surface mass convergence and column moisture convergence. We will return to the subject of above-surface moisture at the end of this section.

We have noted in section 3 that the AGCMs tend to place the maximum of precipitation close to the maxi-

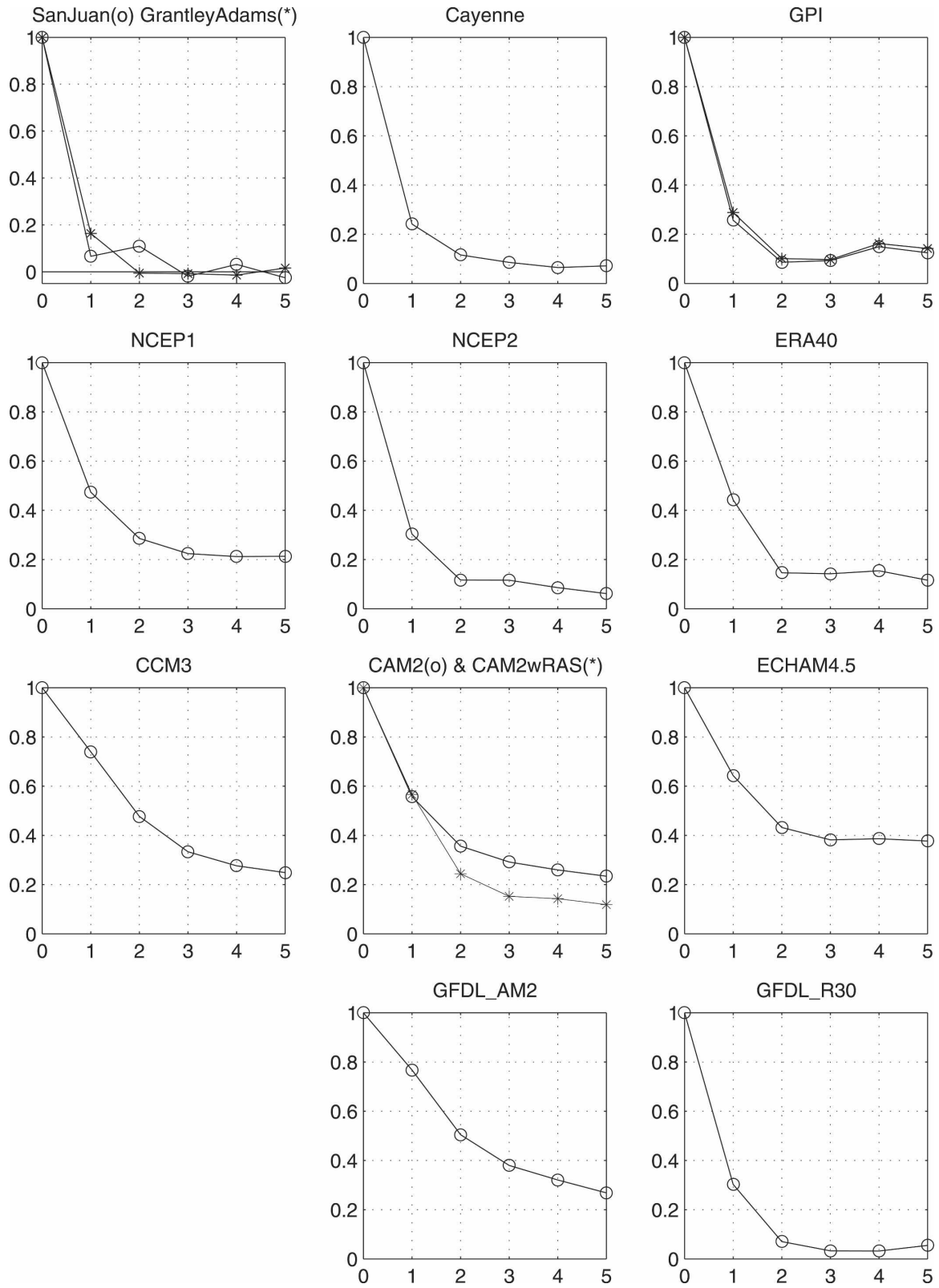


FIG. 8. Autocorrelation of daily precipitation in the AMI region (2° – 10° N across the span of the Atlantic, calculated on days 180–365) as a function of lag (days). The two lines in the GPI box (upper right) correspond to data points with the original resolution (open circle) and the data points regridded at the NCEP2 resolution (stars).

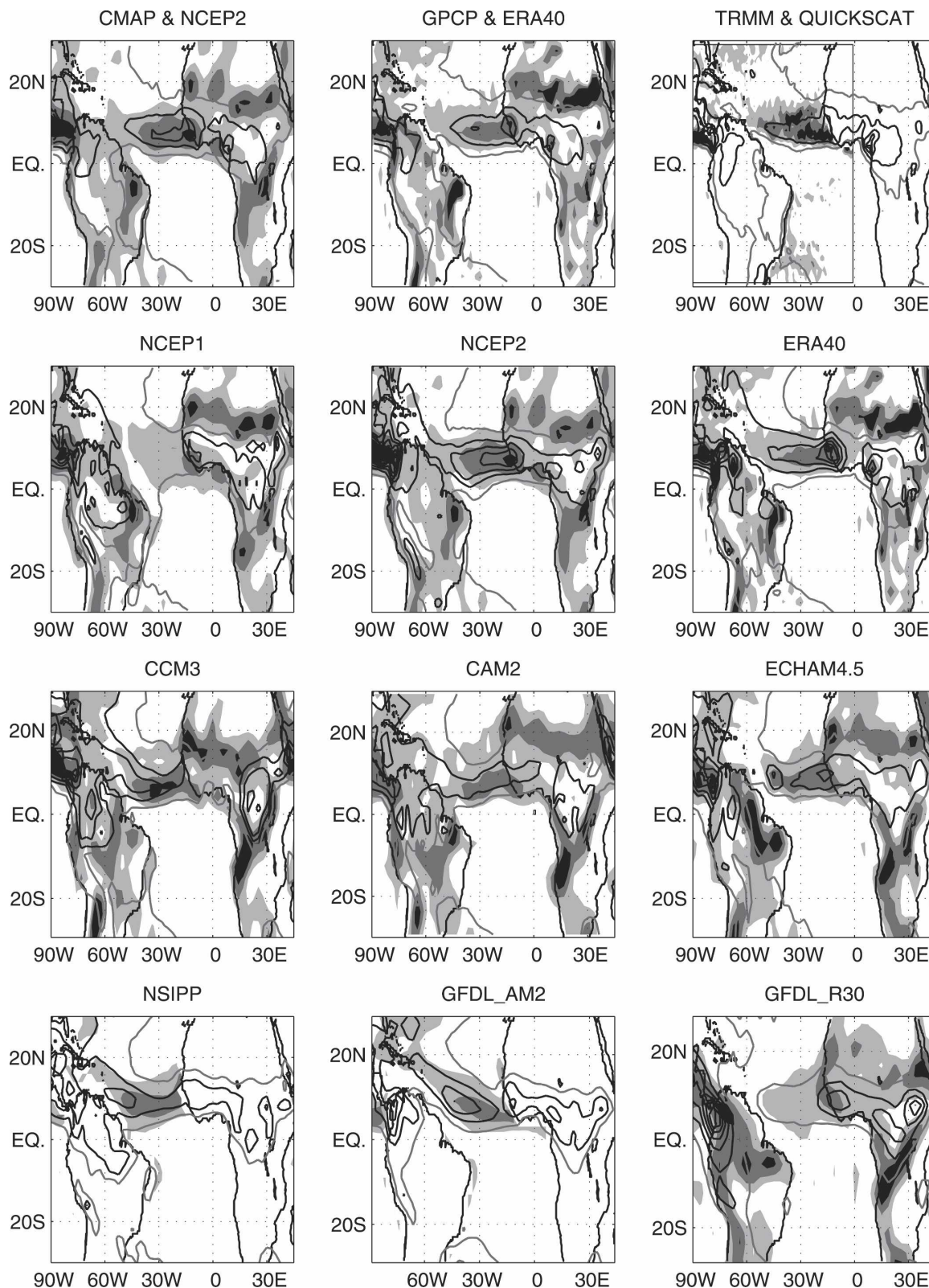


FIG. 9. Climatological September convergence at the surface or at 1000 hPa (shaded, the shading interval is $4 \times 10^{-6} \text{ m s}^{-2}$, only positive convergence is shaded, with darker shading indicating stronger convergence) and precipitation (contours; the contour interval is 4 mm day^{-1} , starting at the 2 mm day^{-1} contour). The convergence field is not accurately calculated near orography.

imum of SST, to an extent not found in observations. We add here that in all datasets—observations, reanalyses, and models—SST is the main factor controlling the distribution of surface moist static energy, h_s , which is maximum where SST is maximum: over the Caribbean in September and in the Gulf of Guinea and offshore from Northeast Brazil in March (not shown). At odds with simple models of tropical precipitation [such as, e.g., that of Sobel and Bretherton (2000), in the cases where they ignored horizontal moisture advection] the observed precipitation at each point is not uniquely determined by the local surface moist static energy, and thus not by the local SST either.

Many explanations that remain consistent with the view of thermodynamic control of precipitation can be invoked for the lack of better correspondence between h_s and precipitation, such as the role of the free-tropospheric temperature and humidity, or the importance of low convective inhibition as another requirement for deep convection (e.g., Yu and Neelin 1997; Mapes 1997; Raymond et al. 2003). Behind these explanations is the fundamental notion that as a parcel of air leaves the surface in a convective updraft, its buoyancy is affected by the characteristics of the environmental air around it. Thus, in the remainder of this section and the following section, we'll bring our attention to the simulated relationship between precipitation and the vertical profiles of moisture and temperature.

Figure 10 shows latitude–pressure cross sections of relative humidity and pressure vertical velocity (ω) in the central Atlantic for the climatological September. As expected, we see that in all datasets ascent is aligned with the humidity maximum at all levels. If ascent is displaced from its observed position, so is the maximum humidity, but the humidity profile at the center of the convective region is reasonably well reproduced (although NSIPP simulates an unusually dry boundary layer, and GFDL_R30 an unusually dry midtroposphere). The most remarkable feature that distinguishes the AGCMs from the NCEP2 and ERA-40 reanalyses is the dryness of the lower troposphere in the subsidence region north of the ITCZ (while we are only showing September relative humidity, the same feature is just as pronounced during March and in the specific humidity field). The result is an excessively sharp gradient in low-level relative humidity across the convection/subsidence boundary to the north of the ITCZ in all AGCM, aside NSIPP (e.g., the drop in relative humidity at about 850 mb between 8° and 20°N equals, in September, 27% for NCEP2, and 49% for CCM3 and CAM2). As an aside, we remark that the drier subsidence zone at about 10°–20°N is not associated with overestimated subsidence, but rather with a

deeper subsidence, and a less developed shallow circulation (cf. Zhang et al. 2004). In the next section we will address whether a drier boundary layer in the upstream region is likely to affect the ITCZ in these models.

Finally, we note that some models, namely CCM3, NSIPP, and the GFDL_R30, simulate shallower ascent than the reanalyses, and all models simulate an ascent profile that is more bottom heavy than that in the reanalyses. This latter feature is unique to the ITCZ: in the Caribbean, both models and reanalysis put maximum ascent at about 400 hPa (but models fail to capture the low-level descent, not shown).

While the depth of convection can explain biases in the position of minimum relative humidity in the upper troposphere, we can hypothesize that tropospheric humidity would also affect the depth of the convection: excessive dryness being carried down to the lower troposphere in the trades region might reduce the intensity of convection in the ITCZ. At the very least, we can expect that the excessive dryness of the boundary layer plays a role in the above-mentioned disconnect between surface mass convergence and column-integrated moisture convergence. The next section explores the relationship between rainfall and humidity in more detail.

5. The local relationship between precipitation and the environment

If convection is the release of an instability, then precipitation at any given point is, to first order, a function of the local vertical profile of temperature and humidity. In this section, we take a close look at the simulated relationship between precipitation and its environment. To do so, inspired by Bretherton et al. (2004), we organize the data according to the amount of precipitation, and not according to geography or seasonality: geography and seasonality are assumed to be acting on convection solely through their action on the large-scale environment.

In Fig. 11, we take a look at how the vertical profiles of temperature and humidity differ in dry and rainy conditions. Here, temperature and humidity are combined in potential temperature, equivalent potential temperature—calculated neglecting the contribution from liquid water (Emanuel 1994)—and saturated equivalent potential temperature. In our computation, we have used daily data, yet we expect that the difference in vertical profiles for rainy and dry days reflects climatological differences, more than day-to-day variability.

The reanalyses show that rain is associated with warmer boundary layer temperatures, but that tem-

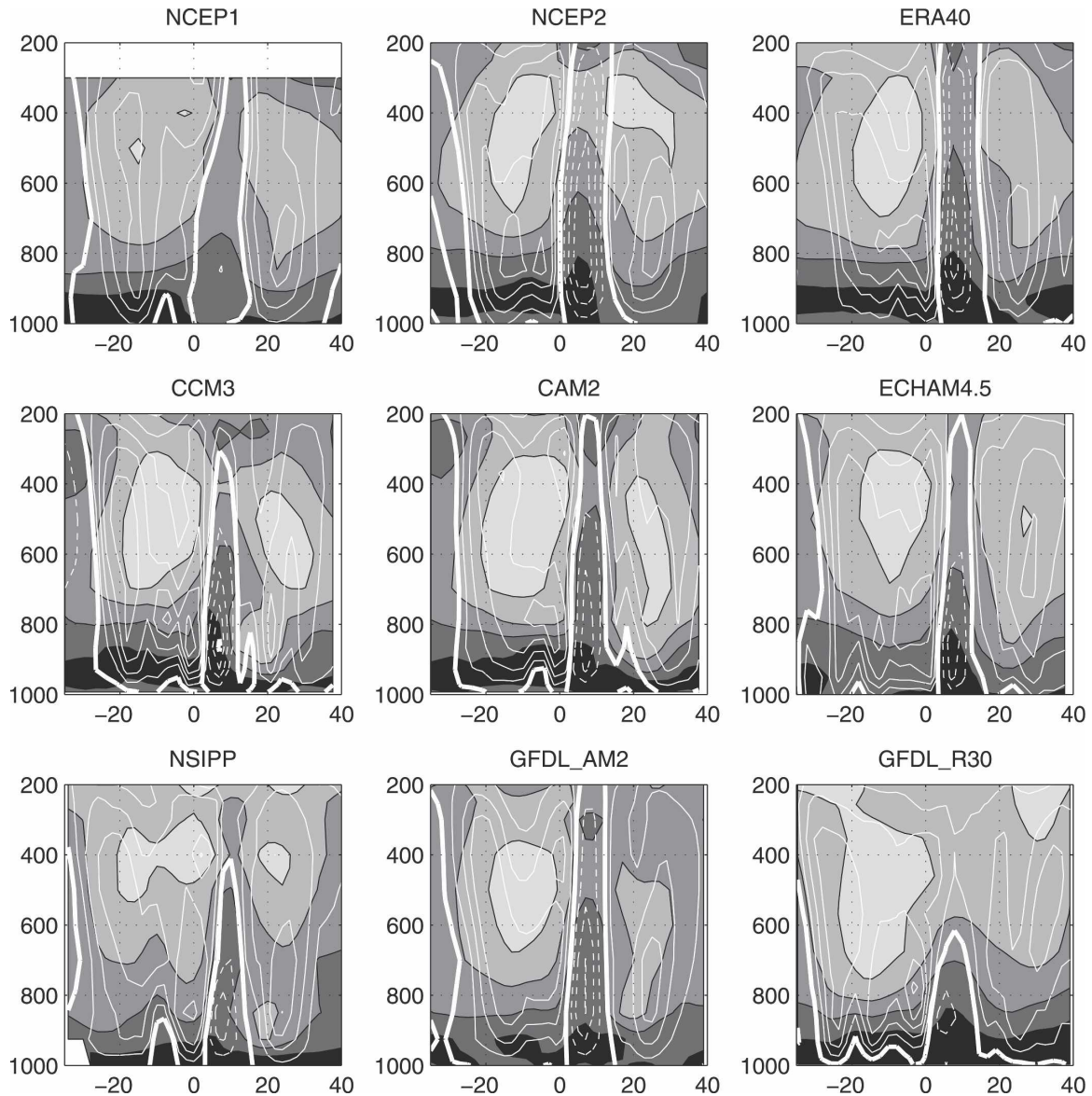


FIG. 10. Climatological September relative humidity (shaded; shading interval is 20%, the darkest shading indicates RH greater than 80%, the lightest indicates RH less than 20%) and vertical velocity (contoured in white; contour interval is 0.01 Pa s^{-1} for positive, downward, values, and 0.025 Pa s^{-1} for negative, upward, values) as a function of pressure and latitude in the central Atlantic (30°W).

perature in the free troposphere is the same, independent of rainfall, consistent with the weak temperature gradient view of the Tropics (Sobel and Bretherton 2000). This pattern is overall well reproduced, but three of the models (CCM3, CAM2wRAS, and GFDL_R30) tend to simulate a slightly cooler free troposphere in presence of rain. The treatment of moisture is somewhat more variable. All models simulate a moister free troposphere under rainy conditions, but some (ERA-40, ECHAM4.5, GFDL_AM2) do so more than others do. Furthermore, models disagree in their treatment of the surface layer humidity: most models simulate either

the same surface humidity in dry and rainy conditions, or a minutely drier surface for rainy conditions (in the three reanalyses, CCM3, and ECHAM4.5 the equivalent potential temperature at the surface is increased from dry to rainy conditions by either the same amount as the potential temperature—indicating no change in moisture, or less—indicating a small reduction in moisture), but in other models (CAMwRAS and GFDL_R30) the surface layer is substantially drier in rainy conditions and in GFDL_AM2 the surface layer is moister in rainy conditions. We have done the same calculation for station data from Caribbean Islands and

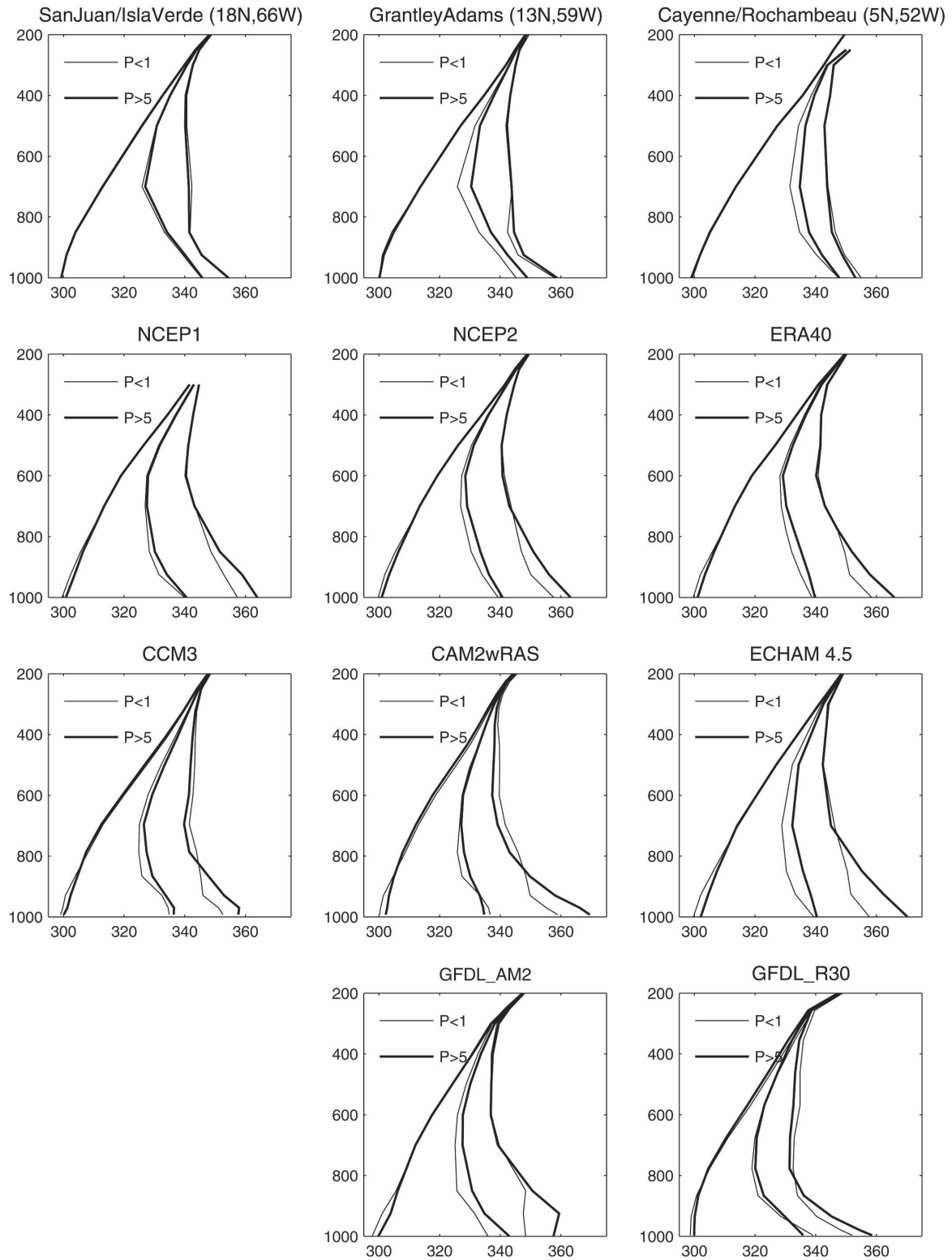


FIG. 11. Vertical profiles of potential temperature, equivalent potential temperature, and saturated equivalent potential temperature (left to right in each plot) binned according to the value of local precipitation and then averaged over all data points with precipitation less than 1 mm day^{-1} (thin line) and greater than 5 mm day^{-1} (thick line). For the reanalyses and models, we have used one year (1999) of daily data at ocean grid points in the region 15°S – 20°N , 50°W – 10°E . For observations, we have used daily data for 1994–99.

coastal South America (Fig. 11, upper panels). These datasets show virtually no change in the potential temperature profile for rainy or dry conditions; they show an inconsistent change in surface humidity, but the expected moistening of the free troposphere for rainy conditions. In particular, they do not show that high precipitation amounts are associated with warmer surface temperature; such behavior might be explained by the fact that these are soundings over land and the surface warming that precedes rain over land and the cooling that follows it are averaged out in the daily data. Surprisingly, the observed profiles also indicate a lower atmosphere closer to saturation than it is in the ITCZ of any reanalysis or model. Unfortunately, we lack the oceanic observations needed to determine which of the various modeled behaviors is correct, if any.

Figure 12 shows the lead-lag correlation between precipitation at the surface and specific humidity throughout the troposphere; correlations are calculated, for models and reanalyses, on an eight-month-long (May–November) daily time series for all grid points at the AMI location (2° – 12° N), and then averaged over all grid points. The choice of domain was made to minimize the contributions of regions of subsidence to the correlations. (The same calculations done over larger domains and for the entire year give nearly identical results. Data points in the Caribbean region show quantitatively different correlations, but the substance of our results does not change.) In lieu of observations in the AMI, we use radiosonde observations at two island locations in the Caribbean and a coastal location in French Guiana. Correlations are calculated over the rainy season (day 180–365), and averaged over six rainy seasons (1994–99). Because the observations describe conditions at individual stations and not over larger spatial scales, we expect the observed relationships to be noisier than the modeled ones.

First, we note how, as should be expected, models that overestimate the autocorrelation of precipitation also overestimate its correlation with humidity for long lead and lag times. Note in particular that correlations for station data are much smaller than for the reanalyses and models (observed correlations have been doubled before being plotted in Fig. 12).

Second, we note in both models and observations a tendency (admittedly neither very sharp nor robust) for greater correlations between precipitation and lower-level humidity when humidity leads, and greater correlations between precipitation and upper-level humidity when precipitation leads. Such a relationship would be consistent with the expectation that deep convection occurs for high boundary layer and lower-troposphere

humidity (moist static energy), and subsequently detains moisture in the free troposphere, and is also consistent, for example, with observations over the tropical oceans (Sherwood and Wahrlich 1999; Straub and Kiladis 2002, 2003; Sobel et al. 2004). We suppose the relationship would become more evident at time scales shorter than daily, but we lack the data to verify as much.

Third, we note a peculiar pattern of correlation in CCM3 and, to a much lesser extent, GFDL_AM2 and CAM2wRAS: correlations between precipitation and humidity have a strong minimum in a layer just above the surface. This pattern of correlation indicates that the surface humidity is decoupled from humidity in the layers just above the surface,³ and that precipitation responds, in these models, primarily to surface humidity. In contrast, the reanalyses show that the maximum correlation occurs at or above the 850-mb level, consistent with some control of deep convection by humidity in the free troposphere (e.g., Sherwood 1999). This might indicate a more prominent role for entrainment in determining the intensity of precipitation in the reanalyses. The precipitation/humidity observed correlation in the Caribbean Islands and the South American coast is different; it is weaker and it increases with height until the top of convection. The latter might be a consequence of the fact that these are land sites, and the diurnal cycle of temperature (not captured by the daily averages used here) is expected to have a stronger control on stability and convection than humidity alone.

At what level of atmospheric humidity does deep convection start and rainfall result? Figure 13 shows the joint distribution of monthly rainfall and total column water vapor (a proxy for lower-tropospheric vapor). In observations, substantial rainfall occurs only if the column humidity exceeds about 40 mm; precipitation increases exponentially with increasing humidity. All reanalyses and models capture the exponential behavior. The most recent reanalyses capture the humidity threshold as well, but the slope of the exponential curve is not well captured—as would be expected, given the wet bias of both reanalyses.

In contrast, most models tend to rain for column humidity that is considerably too low, with the notable

³ This is confirmed by the lead-lag correlation between surface humidity and humidity at higher levels. Observations and the new reanalyses show that correlations with the surface decrease with height, and become insignificant for longer lead-lag times the further from the surface; in contrast, CCM3 and, to a much lesser degree, CAM2wRAS and GFDL_AM2 show no correlation at any lag between surface humidity and humidity in the levels just above.

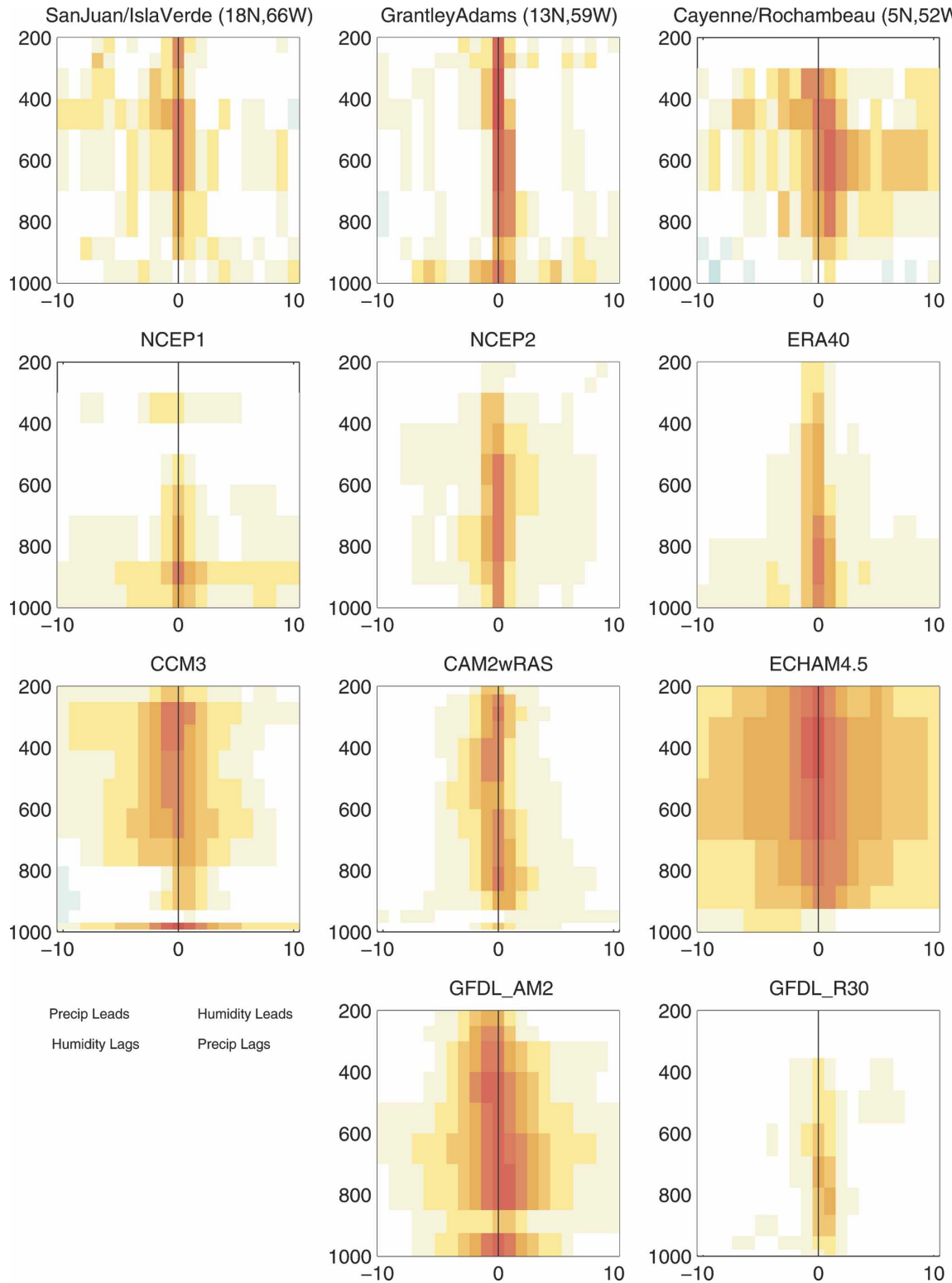


FIG. 12. Lead-lag correlation between precipitation at the surface and specific humidity, as a function of pressure level (hPa) and lead-lag time (days). Correlations are calculated for days 180–365 in 1999 and averaged over all grid points in the Atlantic between 2° and 12°N in the case of reanalyses and GCMs. Correlations are calculated for days 180–365 for each year 1994–99 and then averaged together in the case of the station data. Observed correlations are multiplied by 2. The color axis goes from -0.8 to 0.8, with negative values in blue and positive values in red.

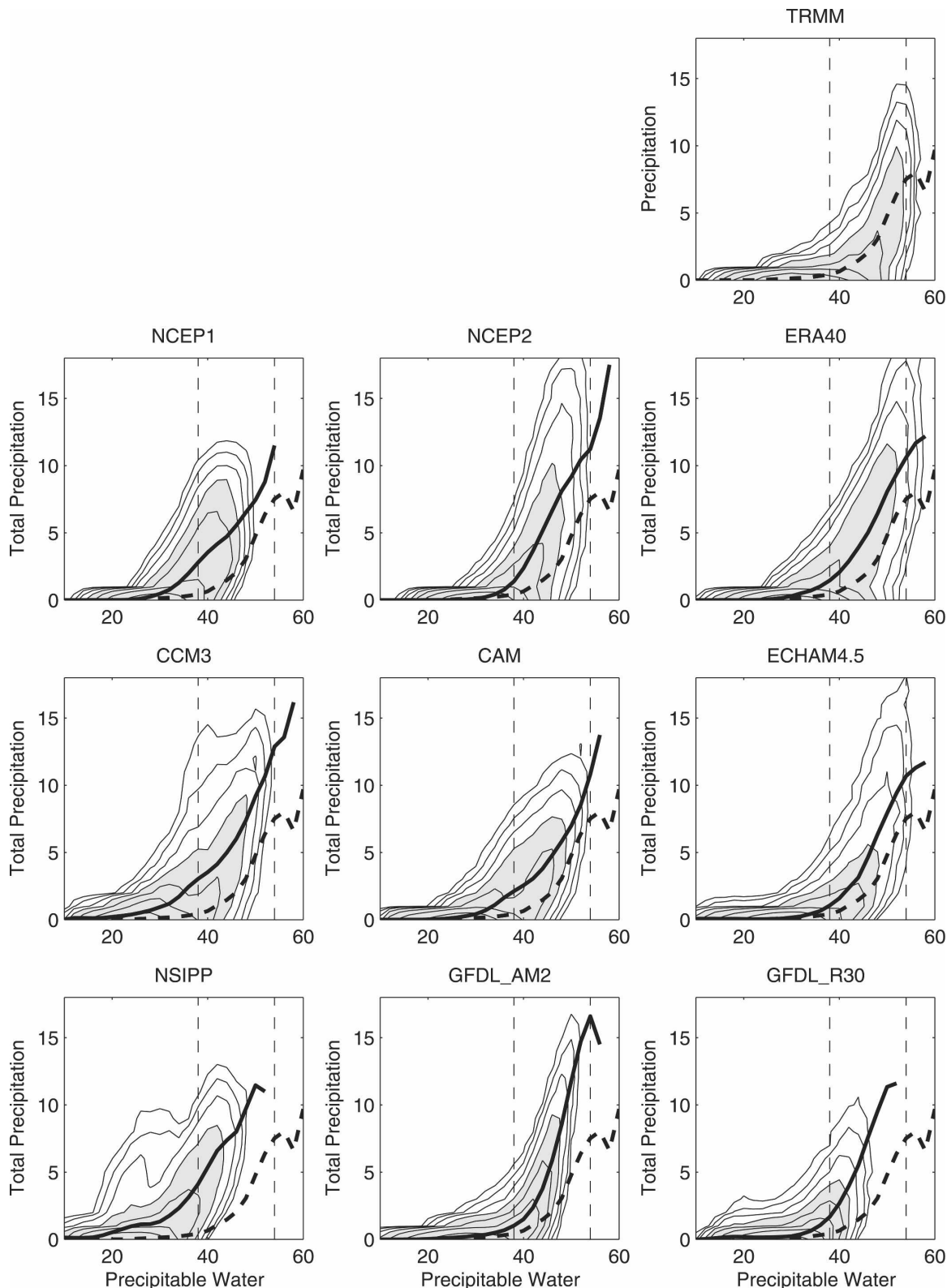


FIG. 13. Normalized joint probability density function for monthly mean precipitation and precipitable water. Only ocean points in the region 20°S–20°N, 70°W–20°E were used; all available months were used. The thick lines represent the mean of the distribution for the models (solid line) and the TRMM dataset (dashed line). The thin, vertical lines indicate the minimum value of precipitable water for which the TRMM dataset exhibits mean precipitation (dashed) and the maximum value of precipitable water at times of no rain.

exception of ECHAM4.5. Both the very low humidity threshold and the sloping right edge of the distribution (best visible in the daily data, not shown) indicate that these models cannot sustain high column humidity, and instead tend to rain prematurely. It is no surprise, then, that these models fail to reproduce the true range of daily rainfall amount, as was shown in Fig. 7.

Finally, in Fig. 14 we show the joint distribution of monthly rainfall and SST. In the TRMM observations, rainfall occurs for SST larger than 26°C, increases linearly until the SST reaches 28°C, and then levels off. The other observational datasets suggest a similar behavior, but with a more gradual increase for cool SST and a tendency to decreasing rainfall for very warm SST. Among the models, the local relationship between rainfall and SST varies more widely. The CCM3 and CAM2 models show a remarkably linear relationship, as we would have expected from the strict correspondence in the rainfall and SST patterns shown in Figs. 2 and 3. The NSIPP and GFDL_AM2 models instead show a sharp decline in rainfall for SST warmer than about 28°C. This is consistent with the fact that, in both these models, rainfall, while biased toward the local maximum of SST, does not mimic the SST pattern as closely (see, e.g., how the maximum September precipitation, while biased toward the western basin, does not reach into the Caribbean; Fig. 3).

6. Summary and conclusions

This study describes the annual cycle of precipitation in the tropical Atlantic basin and compares the available observations to three reanalysis products (the first and second reanalyses from NCEP and ERA-40 from ECMWF) and the simulations of five general circulation models forced with the time series of observed SST and one flux-adjusted coupled GCM. Our focus is on evaluating the GCMs' simulations. A succinct summary of our findings is offered in Table 2. As one would expect, at zeroth order, the annual march of the ITCZ can be described as following the north–south seasonal march of the warmest SST, with substantial rainfall occurring only for SST warmer than about 27°C. At the same time, the Atlantic warm pools are not characterized by large precipitation. In March, the SST is warmest in the Gulf of Guinea, but rainfall is maximum off the Brazilian coast; in September the SST is warmest in the Caribbean Sea, but rainfall is maximum in the eastern basin.

The most recent reanalyses overestimate tropical Atlantic rainfall by roughly 50%, but capture the location of the rainfall maximum quite accurately. Atmospheric

GCMs simulate the intensity of the ITCZ rainfall better, but they have much worse biases in their simulations of the annual march of the ITCZ. During boreal winter and spring AGCMs tend to bring the ITCZ too far into the Southern Hemisphere and in some cases produce a spurious second rainfall maximum in the Gulf of Guinea. During boreal summer and fall they grossly overestimate rainfall in the Caribbean region and in some cases fail to produce a well-defined ITCZ that stretches from Africa into the eastern Atlantic. An exception is ECHAM4.5, which—even if not free from biases, both in the mean ITCZ intensity and especially in the characteristics of daily rainfall—is quite accurate in its placement of the maximum rainfall.

There seems to be an overarching reason for the widespread AGCMs' biases: an excessive sensitivity to the direct forcing from the local SST. The majority of the models considered here place the rainfall maximum squarely over a local SST maximum. This occurs even as these AGCM accurately place the maximum surface wind convergence away from the SST maximum, at the location where the observed ITCZ lies. We interpret this result as follows: monthly mean surface convergence is determined by the meridional wind component, which in turn is mostly determined by surface boundary conditions through a Lindzen and Nigam (1987) mechanism that is well captured by the models. This is consistent with the results of Chiang et al. (2001) who found that this mechanism is more important for the meridional wind than the zonal wind (and thus more likely to determine convergence in regions of large meridional SST gradient where most convergence is meridional), and not inconsistent with Bacmeister and Suarez (2002) who found that the Lindzen–Nigam mechanism was less important than forcing of the surface wind by deeper pressure gradients, but only examined the zonal component of the flow. Yet, in most models convection responds to dynamic lifting and moistening in the boundary layer less than it responds to thermodynamic convective available potential energy (CAPE) generation in the surface layer over high SST, thus the tendency to lay maximum rainfall over the local SST maximum and not over the maximum surface convergence.

We have explored the relationship between precipitation and the vertical profile of humidity by looking at the large-scale, monthly mean fields and at the statistical relationship between the two fields at daily time scales. The monthly mean precipitation and humidity maxima track each other in both reanalyses and GCMs: in the ITCZ region, relative humidity is higher than 80% at the surface and drops off with height more

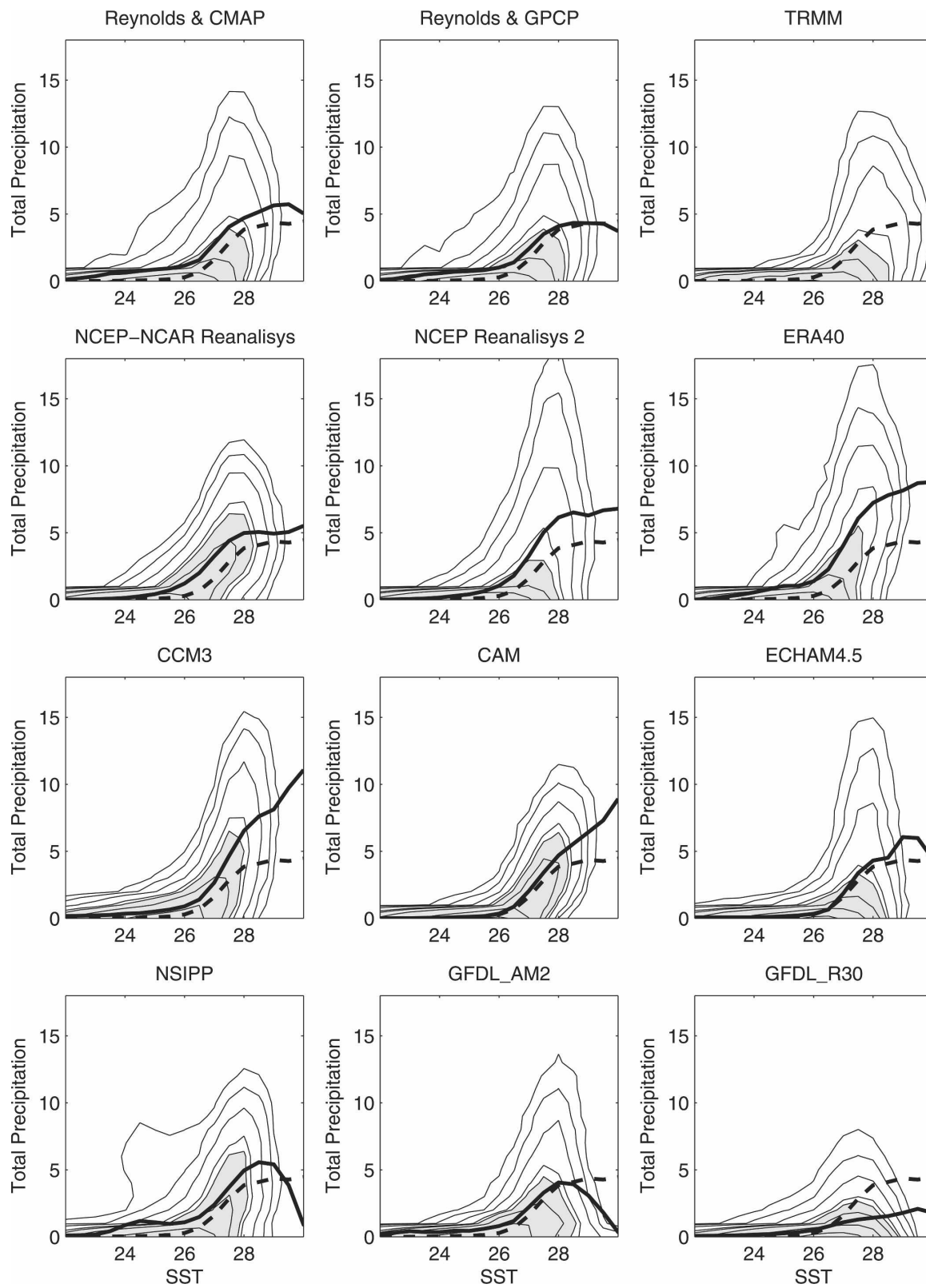


FIG. 14. Normalized joint probability density function for monthly mean precipitation and SST. Only ocean points in the region 20°S–20°N, 70°W–20°E were used; all available months were used. The thick lines represent the mean of the distribution for the models (solid line) and the TRMM dataset (dashed line).

TABLE 2. Summary of model bias in the following areas: the monthly mean rainfall in the ITCZ, the monthly mean $P-E$ in the Caribbean, the characteristics of daily precipitation in the ITCZ, and the large-scale environmental variables. Good performance is indicated by italics. (In the case of the meridional gradient of atmospheric humidity good performance is defined as agreement with the reanalyses.)

Model	ITCZ max	Spring	Summer	Summer	Daily P histogram	$P > 30$ mm events	Daily P spectrum	$\nabla \bullet u_{sfc}$	Sharp $\partial_{lat} q$
		ITCZ south	Caribbean $P > ITCZ P$	Caribbean $P > E$				Max and P max overlap	
NCEP1	<Obs	Yes	Yes	Yes	Flat	No	<i>Weakly red</i>	No	<i>No</i>
NCEP2	>Obs	<i>Weakly</i>	<i>No</i>	Yes	<i>~Obs</i>	<i>Yes</i>	<i>~Obs</i>	<i>Yes</i>	<i>No</i>
ERA-40	>Obs	<i>No</i>	<i>No</i>	Yes	Flat	<i>Yes</i>	<i>Weakly red</i>	<i>Yes</i>	<i>No</i>
CCM3	<i>~Obs</i>	Yes	Yes	Yes	Flat	No	Red	No	Yes
CAM2	<Obs	Yes	<i>Weakly</i>	<i>No</i>	Flat	No	Red	<i>Partial</i>	Yes
CAM2wRAS	<Obs	Yes	Yes	<i>No</i>	<i>~Obs</i>	No	Red	No	Yes
ECHAM4.5	<i>~Obs</i>	<i>Weakly</i>	<i>No</i>	<i>No</i>	<i>~Obs</i>	<i>Yes</i>	Red	<i>Yes</i>	Yes
NSIPP	<Obs	Yes	Yes	Yes	N/a	N/a	N/a	<i>Partial</i>	<i>Weakly</i>
GFDL_AM2	<i>~Obs</i>	Yes	<i>Weakly</i>	<i>No</i>	Flat	No	Red	<i>Partial</i>	<i>Weakly</i>
GFDL_R30	\leq Obs	<i>No</i>	<i>No</i>	<i>No</i>	Peaked	<i>Yes</i>	<i>~Obs</i>	<i>Yes</i>	<i>No</i>

slowly than outside the ITCZ. The AGCMs overestimate the humidity gradient to the north of the ITCZ, and place a sharp humidity minimum below the 800-hPa level at 20°N.

The lead/lag correlation between daily precipitation and humidity profiles indicates that most models are much less sensitive to humidity in layers just above the surface than they are to humidity at the surface. This could be due to an excess of convective mass flux occurring in parameterized updrafts with very low entrainment rates. Analysis of cloud-resolving models shows entrainment rates much larger than those used in typical convective parameterizations (Derbyshire et al. 2004; Kuang and Bretherton 2006) and this has been implicated in biases in GCM simulations of the Madden-Julian oscillation (Tokioka et al. 1988; Lee et al. 2003).

Models that present a weak response to lower-troposphere humidity tend to bias Atlantic precipitation in the following ways. First, as we have mentioned above, the thermodynamic forcing of convection is determined in these models by the surface layer, with the consequence that maximum precipitation is erroneously placed over maximum SST. Second, a smaller amount of water vapor in the atmospheric column is necessary to initiate convection, with the consequence that there are more rainy events for lower precipitable water in the atmospheric column and fewer heavy-rain events, making the distribution of daily rainfall amount flatter than observed. Thus, the way a model simulates the relationship between precipitation and atmospheric humidity appears to affect both steady (monthly mean position) and transient (distribution of daily rainfall) characteristics of the precipitation field. This surprising result follows: models that are oversensitive to SST un-

derestimate the number of days with high rain accumulation.

A consistent picture is emerging from this diagnostic study, that of an Atlantic ITCZ driven by both thermodynamic and dynamic forcings, and quite sensitive to the humidity in the lower troposphere. Models simulate the dynamic forcing well. The sources of bias are the oversensitivity to the thermodynamic forcing in the presence of very warm SST and the lack of sensitivity to humidity above the surface layer.

Acknowledgments. We wish to express our thanks to all the people who have made their model output and observational datasets available to us. We acknowledge Naomi Naik (LDEO) for the CCM3 simulation, R. Saravanan (CGD, NCAR) for CAM2, Eric Maloney (OSU) for CAM2wRAS, and David DeWitt (IRI) for ECHAM4.5. Output for the NSIPP and GFDL models and ERA-40 reanalysis were obtained from their respective Websites (<http://nsipp.gsfc.nasa.gov>, <http://data1.gfdl.noaa.gov>, and <http://data.ecmwf.int/data/>). NCEP Reanalysis 2 data provided by the NOAA-CIRES Climate Diagnostics Center, Boulder, Colorado, USA, from their Web site at <http://www.cdc.noaa.gov/>. Wind data are obtained from the NASA/NOAA-sponsored data system Seaflux, at JPL through the courtesy of W. Timothy Liu and Wenqing Tang. The Distributed Active Archive Center (Code 902) at the Goddard Space Flight Center, Greenbelt, MD 20771, provided the GPI data (produced by Drs. Phillip Arkin and John Janowiak of the Climate Analysis Center, NOAA, Washington, D.C., Goddard's contribution to these activities was sponsored by NASA's Earth Science Enterprise program). CARDS data were downloaded from <http://www.ncdc.noaa.gov/>. The NCEP1,

CMAP, GPCP, and station precipitation data were obtained through the data library at IRI (<http://ingrid.lidgo.columbia.edu/>).

REFERENCES

- Adler, R. F., G. J. Huffman, D. T. Bolvin, S. Curtis, and E. J. Nelkin, 2000: Tropical rainfall distributions determined using TRMM combined with other satellite and rain gauge information. *J. Appl. Meteor.*, **39**, 2007–2023.
- , and Coauthors, 2003: The Version-2 Global Precipitation Climatology Project (GPCP) monthly precipitation analysis (1979–present). *J. Hydrometeorol.*, **4**, 1147–1167.
- Anderson, J. L., and Coauthors, 2004: The new GFDL global atmosphere and land model AM2/LM2: Evaluation with prescribed SST simulations. *J. Climate*, **17**, 4641–4673.
- Arakawa, A., 2004: The cumulus parameterization problem: Past, present, and future. *J. Climate*, **17**, 2493–2525.
- Bacmeister, J. T., and M. J. Suarez, 2002: Wind stress simulations and the equatorial momentum budget in an AGCM. *J. Atmos. Sci.*, **59**, 3051–3073.
- , P. J. Pegion, S. D. Schubert, and M. J. Suarez, 2000: Atlas of seasonal means simulated by the NSIPP1 atmospheric GCM. NASA Tech. Memo-2000-104606, Vol. 17, 194 pp.
- Biasutti, M., 2000: Decadal variability in the tropical Atlantic as simulated by the climate system model and the CCM3 coupled to a slab ocean model. M.S. thesis, Dept. of Atmospheric Sciences, University of Washington, 43 pp.
- , D. S. Battisti, and E. S. Sarachik, 2005: Terrestrial influence on the annual cycle of the Atlantic ITCZ. *J. Climate*, **18**, 211–228.
- Bretherton, C. S., M. E. Peters, and L. E. Back, 2004: Relationships between water vapor path and precipitation over the tropical oceans. *J. Climate*, **17**, 1517–1528.
- Charney, J., 1971: Tropical cyclogenesis and the formation of the intertropical convergence zone. *Mathematical Problems in Geophysical Fluid Dynamics*, W. H. Reid, Ed., Vol. 13, *Lectures in Applied Mathematics*, American Mathematical Society, 355–368.
- Chiang, J., S. Zebiak, and M. Cane, 2001: Relative roles of elevated heating and surface temperature gradients in driving anomalous surface winds over tropical oceans. *J. Atmos. Sci.*, **58**, 1371–1394.
- Da Silva, A., A. C. Young, and S. Levitus, 1994: NOAA SMD94. Tech. Rep. 6, U.S. Dept. of Commerce, NOAA, NESDIS, 83 pp.
- Davey, M. K., and Coauthors, 2002: STOIC: A study of coupled model climatology and variability in tropical ocean regions. *Climate Dyn.*, **18**, 403–420.
- Delworth, T. L., R. J. Stouffer, K. W. Dixon, M. J. Spelman, T. R. Knutson, A. J. Broccoli, P. J. Kushner, and R. T. Wetherald, 2002: Review of simulations of climate variability and change with the GFDL R30 coupled climate model. *Climate Dyn.*, **19**, 555–574.
- , and Coauthors, 2006: GFDL's CM2 global coupled climate models. Part 1: Formulation and simulation characteristics. *J. Climate*, **19**, 643–674.
- Derbyshire, S., I. Beau, P. Bechtold, J.-Y. Grandpeix, J.-M. Piriou, J. Redelsperger, and P. Soares, 2004: Sensitivity of moist convection to environmental humidity. *Quart. J. Roy. Meteor. Soc.*, **130**, 3055–3079.
- DeWitt, D., 2004: Diagnosis of the tropical Atlantic near equatorial SST bias in a directly coupled atmosphere–ocean general circulation model. *Geophys. Res. Lett.*, **32**, L01703, doi:10.1029/2004GL021707.
- Emanuel, K. A., 1994: *Atmospheric Convection*. Oxford University Press, 580 pp.
- , J. Neelin, and C. Bretherton, 1994: On large-scale circulations in convecting atmospheres. *Quart. J. Roy. Meteor. Soc.*, **120**, 1111–1143.
- Eskridge, R. E., O. A. Alduchov, I. V. Chernykh, Z. Panmao, A. C. Polansky, and S. R. Doty, 1995: A Comprehensive Aerological Reference Data Set (CARDS): Rough and systematic errors. *Bull. Amer. Meteor. Soc.*, **76**, 1759–1775.
- Goddard, L., and S. Mason, 2002: Sensitivity of seasonal climate forecasts to persisted SST anomalies. *Climate Dyn.*, **19**, 619–632, doi:10.1007/s00382-002-0251-y.
- , —, S. Zebiak, C. Ropelewski, R. Basher, and M. A. Cane, 2001: Current approaches to seasonal-to-interannual climate predictions. *Int. J. Climatol.*, **21**, 1111–1152.
- Graf, J. E., W. Yang Tsi, and L. Jones, 1998: Overview of QuikSCAT mission—A quick deployment of a high resolution, wide swath scanning scatterometer for ocean wind measurement. *Proceedings IEEE Southeastcon*, Engineering for a New Era (Cat. 98CH36170), 314–317.
- Hack, J., 1994: Parameterization of moist convection in the National Center for Atmospheric Research Community Climate Model (CCM2). *J. Geophys. Res.*, **99**, 5551–5568.
- Holton, J. R., J. M. Wallace, and J. M. Young, 1971: On boundary layer dynamics and the itcz. *J. Atmos. Sci.*, **28**, 275–280.
- Huang, B., P. Schopf, and J. Shukla, 2004: Intrinsic ocean–atmosphere variability of the tropical Atlantic Ocean. *J. Climate*, **17**, 2058–2077.
- Josey, S. A., E. C. Kent, and P. K. Taylor, 1998: The Southampton Oceanography Centre (SOC) ocean–atmosphere heat, momentum and freshwater flux atlas. Southampton Oceanography Centre Rep. 6, 30 pp. + figs.
- Kalnay, E., and Coauthors, 1996: The NCEP/NCAR 40-Year Reanalysis Project. *Bull. Amer. Meteor. Soc.*, **77**, 437–471.
- Kanamitsu, M., W. Ebisuzaki, J. Woollen, S.-K. Yang, J. J. Hnilo, M. Fiorino, and G. L. Potter, 2002: NCEP DOE AMIP-II reanalysis (R-2). *Bull. Amer. Meteor. Soc.*, **83**, 1631–1643.
- Kiehl, J. T., and P. R. Gent, 2004: The Community Climate System Model, version 2. *J. Climate*, **17**, 3666–3682.
- , J. J. Hack, G. B. Bonan, B. A. Boville, D. L. Williamson, and P. J. Rasch, 1998: The National Center for Atmospheric Research Community Climate Model: CCM3. *J. Climate*, **11**, 1131–1150.
- Kuang, Z., and C. Bretherton, 2006: A mass flux scheme view of a high-resolution simulation of a transition from shallow to deep cumulus convection. *J. Atmos. Sci.*, in press.
- Kumar, A., and M. P. Hoerling, 1998: Specification of regional sea surface temperatures in atmospheric general circulation model simulations. *J. Geophys. Res.*, **103**, 8901–8907.
- Lee, M.-I., I.-S. Kang, and B. Mapes, 2003: Impacts of cumulus convection parameterization on aqua-planet AGCM simulations of tropical intraseasonal variability. *J. Meteor. Soc. Japan*, **81**, 963–992.
- Lindzen, R. S., 1974: Wave-CISK in the Tropics. *J. Atmos. Sci.*, **31**, 156–179.
- , and S. Nigam, 1987: On the role of sea-surface temperature gradients in forcing low-level winds and convergence in the tropics. *J. Atmos. Sci.*, **44**, 2418–2436.
- Manabe, S., J. Smagorinsky, and R. Strickler, 1965: Simulated

- climatology of a general circulation model with a hydrologic cycle. *Mon. Wea. Rev.*, **93**, 769–798.
- Mapes, B. E., 1997: Equilibrium vs. activation control of large-scale variations of tropical deep convection. *The Physics and Parameterization of Moist Atmospheric Convection*, R. K. Smith, Ed., Kluwer, 321–358.
- Moorthi, S., and M. J. Suarez, 1992: Relaxed Arakawa–Schubert: A parameterization of moist convection for general circulation models. *Mon. Wea. Rev.*, **120**, 978–1002.
- Neelin, J. D., 1997: Implications of convective quasi-equilibrium for the large-scale flow. *The Physics and Parameterization of Moist Atmospheric Convection*, R. K. Smith, Ed., Kluwer, 413–446.
- , and I. M. Held, 1987: Modeling tropical convergence based on the moist static energy budget. *Mon. Wea. Rev.*, **115**, 3–12.
- , and H. Su, 2005: Moist teleconnection mechanisms for the tropical South American and Atlantic sector. *J. Climate*, **18**, 3928–3950.
- Nordeng, T. E., 1994: Extended versions of the convective parameterization scheme at ECMWF and their impact on the mean and transient activity of the model in the tropics. ECMWF Tech. Memo. 206, 41 pp.
- Oberhuber, J., 1988: An atlas based on the COADS data set: The budgets of heat buoyancy and turbulent kinetic energy at the surface of the global ocean. Max-Planck-Institut für Meteorologie Rep. 15, 19 pp.
- Raymond, D., 2000: Thermodynamic control of tropical rainfall. *Quart. J. Roy. Meteor. Soc.*, **126**, 889–898.
- , G. Raga, C. Bretherton, J. Molinari, C. Lopez-Carrillo, and Z. Fuchs, 2003: Convective forcing in the intertropical convergence zone of the eastern Pacific. *J. Atmos. Sci.*, **60**, 2064–2082.
- Reynolds, R. W., and T. M. Smith, 1994: Improved global sea surface temperature analyses. *J. Climate*, **7**, 929–948.
- Roeckner, E., and Coauthors, 1996: The atmospheric circulation model ECHAM-4: Model description and simulation of present-day climate. Tech. Rep., MPI für Meteorologie, Hamburg, 90 pp.
- Sherwood, S. C., 1999: Convective precursors and predictability in the tropical western Pacific. *Mon. Wea. Rev.*, **127**, 2977–2991.
- , and R. Wahrlich, 1999: Observed evolution of tropical deep convective events and their environment. *Mon. Wea. Rev.*, **127**, 1777–1795.
- Simmons, A., and J. Gibson, 2000: The ERA-40 Project Plan. ERA-40 Project Report Series 1, ECMWF, 63 pp.
- Sobel, A. H., and C. S. Bretherton, 2000: Modeling tropical precipitation in a single column. *J. Climate*, **13**, 4378–4392.
- , S. Yuter, C. Bretherton, and G. Kiladis, 2004: Large-scale meteorology and deep convection during TRMM KWJEX. *Mon. Wea. Rev.*, **132**, 422–444.
- Straub, K. H., and G. N. Kiladis, 2002: Observations of a convectively coupled Kelvin wave in the eastern Pacific ITCZ. *J. Atmos. Sci.*, **59**, 30–53.
- , and —, 2003: The observed structure of convectively coupled Kelvin waves: Comparison with simple models of coupled wave instability. *J. Atmos. Sci.*, **60**, 1655–1668.
- Tiedtke, M., 1989: A comprehensive mass flux scheme for cumulus parameterization in large-scale models. *Mon. Wea. Rev.*, **117**, 1779–1800.
- Tokioka, T., K. Yamazaki, A. Kitoh, and T. Ose, 1988: The equatorial 30–60 day oscillation and the Arakawa–Schubert penetrative cumulus parameterization. *J. Meteor. Soc. Japan*, **66**, 883–901.
- Tomas, R., and P. Webster, 1997: The role of inertial instability in determining the location and strength of near-equatorial convection. *Quart. J. Roy. Meteor. Soc.*, **123**, 1445–1482.
- , J. Holton, and P. Webster, 1999: The influence of cross-equatorial pressure gradients on the location of near-equatorial convection. *Quart. J. Roy. Meteor. Soc.*, **125**, 1107–1127.
- Waliser, D. E., and R. Somerville, 1994: Preferred latitudes of the intertropical convergence zone. *J. Atmos. Sci.*, **51**, 1619–1639.
- Wentz, F. J., C. Gentemann, D. Smith, and D. Chelton, 2000: Satellite measurements of sea surface temperature through clouds. *Science*, **288**, 847–850.
- Xie, P., and P. A. Arkin, 1997: Global precipitation: A 17-year monthly analysis based on gauge observations, satellite estimates, and numerical model outputs. *Bull. Amer. Meteor. Soc.*, **78**, 2539–2558.
- Yu, J.-Y., and J. Neelin, 1997: Analytic approximations for moist convectively adjusted regions. *J. Atmos. Sci.*, **54**, 1054–1063.
- Zhang, C., M. McGauley, and N. Bond, 2004: Shallow meridional circulation in the tropical eastern Pacific. *J. Climate*, **17**, 133–139.
- Zhang, G., and N. A. McFarlane, 1995: Sensitivity of climate simulations to the parameterization of cumulus convection in the Canadian Climate Centre General Circulation Model. *Atmos.–Ocean*, **33**, 407–446.